

Receiver for Solar Bakery

Submitted in partial fulfillment of the requirements of the

degree of

Master of Technology

by

Ankur Kumar

(Roll no: 213170001)

Supervisor:

Prof. Shireesh B. Kedare



Department of Energy Science and Engineering

INDIAN INSTITUTE OF TECHNOLOGY BOMBAY

June 2023

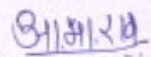
Dissertation Approval Certificate

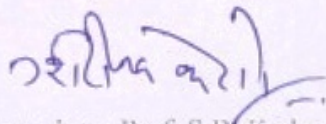
This dissertation entitled "**Receiver for Solar Bakery**" by **Ankur Kumar (213170001)** is approved for the degree of **Master of Technology** with specialization in **Energy Systems Engineering** from Indian Institute of Technology Bombay, India.

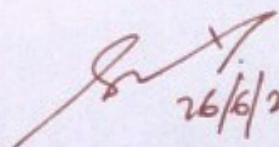
Date: June 26, 2023

Place: DESE, IIT Bombay


Examiner 1: Prof. Santanu Bandyopadhyay


Examiner 2: Prof. Anand B. Rao


Supervisor: Prof. S.B. Kedare



Chairperson: Prof. Santanu Bandyopadhyay

26/6/2023

Declaration

I certify that

- a) The work contained in this report is original and has been done by me under the guidance of my supervisor.
- b) The work has not been submitted to any other Institute for any degree or diploma.
- c) I have followed the guidelines provided by the Institute in preparing the report.
- d) I have conformed to the norms and guidelines given in the Ethical Code of Conduct of the Institute.
- e) Whenever I have used materials (data, theoretical analysis, figures, and text) from other sources, I have given due credit to them by citing them in the text of the report and giving their details in the references. Further, I have taken permission from the copyright owners of the sources, whenever necessary.



Signature

Ankur Kumar

Roll no. 213170001

Date: 21st June, 2023

Abstract

The Indian market for bakery goods is expected to expand at a Compound Annual Growth Rate of 8.5% between 2021 and 2026. Solar thermal technology is getting more attention nowadays and bakery could be one of such application that requires a temperature of 150°C temperature. The study of the bakery process, temperature requirement, and energy requirement is necessary to design and develop of receiver for bakery purposes.

This report presents the numerical 3-dimensional study of heat transfer in a solar receiver designed for bakery applications. The objective of the study was to investigate the temperature distribution and energy requirements and heat losses of different surfaces within the receiver.

The analysis involved studying the temperature variations of cookies, walls, and glass surfaces under different heat inputs (866W, 1000W, and 1135W). The findings demonstrate that the temperature variation of the cookie and walls of the receiver at an input of 1000W closely resembles the experimental results with a deviation of less than 5% for the cookie and 14% for the wall.

The analysis of energy requirements revealed that as the temperature increased, the heat transfer rate decreased, leading to a decrease in the heating energy required. The energy loss in the system was influenced by the surface temperatures, with higher temperatures resulting in increased heat losses. Finally, at a steady state, the heating energy required approached zero, signifying that all input energy was dissipated as heat loss.

Overall, this study provides valuable insights into the heat transfer characteristics of a solar receiver for bakery applications. The findings can inform the design and optimization of solar heating systems, improving energy efficiency and baking performance.

Keywords: Chemistry of baking, heat transfer, system losses, receiver design, Energy requirements, ANSYS fluent

Table of Contents

Abstract.....	iv
List of Figures.....	vii
List of Tables.....	ix
Nomenclature.....	x
1 Introduction	11
1.1 Background of the Project	11
1.2 Objectives	12
1.3 Report Structure	13
2 Review of Literature.....	14
2.1 Baking Process	14
2.1.1 Chemistry of Baking	14
2.1.2 Heat Transfer	16
2.2 Review of receiver design	18
2.2.1 Scheffler dish-based bakery oven.....	18
2.2.2 Solar Fire Lytefire 5	19
2.3 System Losses	20
2.4 Energy and Mass balance in baking chamber.....	21
2.4.1 Thermal analysis of baking process	21
2.4.2 Mass Conservation.....	23
2.4.3 Energy balance.....	23
2.5 Set-up of previous experiment	24
2.6 Experimentally achieved results	25
3 Development of Methodologies	28
3.1 View Factor Calculation using Steady-State Thermal Analysis in ANSYS:.....	28
3.1.1 Introduction:	28
3.1.2 Methodology:	28
3.2 Ray Independence Test using COMSOL.....	34

3.2.1	Collector design	35
3.2.2	Prototype development using COMSOL:	36
3.2.3	Results:.....	37
3.3	Losses In Receiver	38
3.3.1	Radiation Loss Calculations:.....	38
3.3.2	Convective Loss:.....	41
3.4	Energy Balance equation of the receiver.....	44
3.5	Numerical Investigation:.....	44
3.5.1	Description of receiver geometry.....	45
3.5.2	Meshing:	46
3.5.3	Grid dependency test	48
3.5.4	Boundary Conditions	48
3.5.5	Computational model:	49
4	Results and Discussions	50
4.1	Numerical results:.....	50
4.2	Comparison of experimental and numerical results	51
4.2.1	Cookie temperature:.....	51
4.2.2	Wall temperature:	52
4.3	Temperature variation on different surfaces in the receiver	53
4.4	Energy losses and energy absorbed in receiver.....	54
5	Conclusion and Future Plan	58
5.1	Conclusion.....	58
5.2	Future Scope	59
6	References	60

List of Figures

Figure 2.1: Baking process with respect to time (Davidson, I., 2016).....	14
Figure 2.2: Temperature change of biscuits/cookies with respect to time (Davidson, I., 2016).....	15
Figure 2.3 Mineral wool insulation for oven insulation (Davidson, I., 2016)	17
Figure 2.4: Summary of the effects of the modes of heat transfer (Davidson, I., 2016).....	18
Figure 2.5: Scheffler Dish based solar oven(Ayub et al., 2018b)	19
Figure 2.6: Solar Fire Lytefire5 solar oven setup(Lytfire, 2022).....	20
Figure 2.7: Schematic illustrating the progression of air quality at different locations within the solar bakery unit during the baking process. (Ayub et al., 2018a)	21
Figure 2.8: Inlet and outlet conditions of air in baking chamber (Ayub et al., 2018a)	22
Figure 2.9: Actual Setup in field testing (Jagtap, Kedare and Modi, 2021).....	25
Figure 2.10: Temperature rise profile inside cookies (Jagtap, Kedare and Modi, 2022).....	25
Figure 2.11: Average time consumption for different loads (Jagtap, Kedare and Modi, 2022)	26
Figure 2.12: Energy consumption per kg for different loads (Jagtap, Kedare and Modi, 2022)	27
Figure 3.1: Surface 1 is considered in calculating view factors i.e., top wall, bottom wall, right wall, left wall, and back side cylindrical portion	29
Figure 3.2: Surface 2 is considered in calculating view factors i.e., Trays and cookies	29
Figure 3.3: Surface 3 is considered in calculating view factors i.e., Radiation wall.....	29
Figure 3.4: Meshing of Receiver.....	30
Figure 3.5: Collector placed in the Global Coordinate System	36
Figure 3.6: CAD model of receiver of Receiver and collector	37
Figure 3.7: Share of radiative and convective heat transfer loss in receiver.....	43
Figure 3.8: Receiver Geometry	45
Figure 3.9: Meshing of receiver.....	47
Figure 4.1: Temperature contours of receiver at input of 1000W	50

Figure 4.2: Temperature distribution inside receiver	51
Figure 4.3: Comparison of cookie temperature at different heat inputs with experimental value	52
Figure 4.4: Temperature analysis of the wall under varying heat inputs and compared with experimental results	53
Figure 4.5: Variation of temperature on different surfaces of receiver.....	54
Figure 4.6: Variation of Different types of losses in the receiver with heating time	55
Figure 4.7: Variation of heating energy required for cookies, glass and walls with heating time	56
Figure 4.8: Relationship between variation of total heating energy and heat loss with time.....	57

List of Tables

Table 3.1: Temperature input values of different surfaces to solver.....	32
Table 3.2: Radiation values at different surfaces	33
Table 3.3: Percentage of energy falling for different number of rays.....	37
Table 3.4: Values of variables used in equation 3.1	41
Table 3.5: Values of variables used in equation 3.2	43
Table 3.6: Geometrical Dimensions of Receiver	46
Table 3.7: Grid dependency test	48
Table 3.8: Material properties	49

Nomenclature

Q_R	Radiation Loss (W)
σ	Stefan Boltzmann constant ($5.67 \times 10^{-8} \text{ W/m}^2 \cdot \text{K}$)
ε_1	Emissivity of wall
ε_2	Emissivity of glass
F_{12}	View factor of wall with respect to glass
F_{2a}	View factor of glass with respect to ambient
A_1	Surface area of wall (m^2)
A_2	Surface area of glass (m^2)
T_w	Surface temperature of wall (K)
T_g	Surface temperature of glass (K)
Q_C	Convective heat transfer (W)
Q_{absorbed}	Absorbed heat required for heating (W)
h	Heat transfer coefficient ($\text{W/m}^2\text{K}$)
T_{glass}	External surface temperature of glass (K)
T_{air}	Air outlet temp (K)
m_{cookies}	Mass of cookies (kg)
m_{wall}	Mass of steel wall (kg)
m_{glass}	Mass of glass (kg)
m_{air}	Mass flow rate of air (g/sec)
C_p	Specific heat of air (J/g-K)
I_{bn}	Beam radiation (W/m^2)
A_{ap}	Aperture area (m^2)
η_{opt}	Optical efficiency

$\frac{\Delta T}{\Delta t}$	Rate of change of temperature (°C/sec)
β	Collector Frame Inclination w.r.t horizontal (degrees)
ϵ_x	Inclination given to mirror about x-axis (degrees)
ϵ_y	Inclination given to mirror about y-axis (degrees)
Ψ	Rotation given to carrier rods (degrees)
θ_i	Angle of incidence of incoming radiation with mirror normal (degrees)
θ_j	Angle of incidence of reflected rays from mirror with receiver normal (degrees)
θ_z	Solar zenith angle (degrees)

Chapter 1

Introduction

1.1 Background of the Project

Cooking has been majorly consumed in developing nations and hence being a main energy application. Food preparation, particularly baking, requires a lot of energy, which makes it more difficult for developing nations experiencing extreme energy shortages. Due to its flavour, convenience and affordability, a range of bakery items such as bread, biscuits, cookies, and cakes have seen an increase in consumption in India during the last few years (Gruber, 2013).

The market for bakery goods is anticipated to increase from Rs.34 x 10⁵ crores in 2021 to Rs.48 x 10⁵ crores in 2028, expanding at a Compound Annual Growth Rate (CAGR) of 5.12% from 2021 to 2028. The rise of CAGR is due to growing demand for handy meals, rising spending on packaged foods and increasing westernization in the emerging markets (Fortune business insights, 2022). According to the website of Expert Market Research, the value of the Indian bakery industry was estimated to be around Rs.0.62 x 10⁵ crores in 2020. The market is projected to expand at a CAGR of 8.5% between 2021 and 2026, growing to a value of Rs.1 x 10⁵ crores by that time. The region's robust biscuit and cookie business provides assistance for India's bakery industry (Food marketing technology, 2022).

By 2027, the volume in the bread category is anticipated to reach 49,952.5 mkg. In 2023, it's anticipated that the Bread segment will see a volume rise of 5.4%. In the bread category, the average volume per person is anticipated to reach 30.4 kg in 2022 (Statista, 2022).

The popularity of bakery items is a result of their accessibility and low cost. Further driving development is the bread industry's ongoing evolution with the introduction of novel goods. The

expansion of the baked products sector is substantially influenced by the growing popularity of working women, western diets, and urbanisation.

India is the largest consumer and second largest producer of food and due to its food and agriculture sector it has the potential to be the biggest. One of the largest sectors of India's processed food industry is the bakery sector. The majority of baked goods, which include bread and biscuits, are classified as bakery products and account for more than 82 percent of all bakery items produced in the nation. Being the third-largest producer of biscuits, India's bakery industry has a competitive edge in production because to the country's plentiful availability of essential ingredients. Out of all the food production methods, baking calls for the widest variety of processing temperatures. As a result, the bakery uses a significant amount of energy. About 73 percent of the energy required to produce bread is used in the baking process alone (Mishra et al., 2019)

1.2 Objectives

- 1) To enhance the existing design of a solar receiver tailored for bakery applications, utilizing concentrated solar thermal technology, namely the Novel Fresnel Reflector.
- 2) To analyze the temperature distribution and heat transfer within a solar receiver for bakery applications with the help of modelling and simulation of receiver design.
- 3) To evaluate the energy requirements for heating different components of the receiver, such as cookies, glass, and walls.
- 4) To understand the impact of varying heat inputs on the temperature profiles and heating time of the system.
- 5) To investigate the losses of heat energy through convective and radiative mechanisms within the receiver.

1.3 Report Structure

The layout of the report is the following:

Chapter 1: This chapter includes the introduction part which explain project background and the goals of the analysis or research.

Chapter 2: This chapter provides an overview of the literature review conducted for this study. It covers various aspects, including the baking process, a review of different receiver designs, an examination of system losses, and an analysis of energy and mass balance within the baking chamber.

Chapter 3: This chapter includes the methodology to achieve final results like calculation of losses and heat requirements, temperature variation at different surfaces in receiver, energy balance equation and numerical investigation.

Chapter 4: This chapter deals with the results and discussions having comparison between experimental and numerical results, temperature contours and energy losses and energy absorbed in receiver.

Chapter 5: This final chapter has conclusions and future plans related solar bakery.

Chapter 2

Review of Literature

2.1 Baking Process

There are mainly three steps involved while conversion of Dough to bakery item such as biscuit or cookie and they are as follows:

- i. Development of biscuit/cookie structure and texture
- ii. Decrease in the moisture content
- iii. Development of the color

As the baking process goes on there are variations in the dough piece which can be shown in *Figure 2.1*: (Davidson, I., 2016)

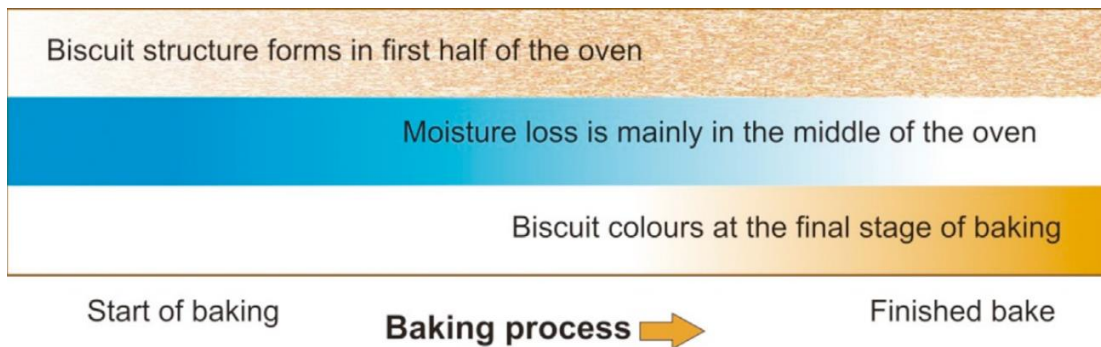


Figure 2.1: Baking process with respect to time (Davidson, I., 2016)

2.1.1 Chemistry of Baking

Development of biscuit/cookies structure and texture

In the biscuit/cookies doughs, various chemical and physical transformations occurs. These changes depend on temperature, heat, humidity of baking chamber and moisture content of dough.

The water in the dough is essential for creating the biscuit's texture and structure because it hydrates the protein, which helps the gluten form and grow, and the starch granules, which cause them to expand and gelatinize. Proteins expand more when heated from 30 to 50 degrees. When the lengthy molecular chains are broken at temp greater than 50°C denaturation of the proteins occurs. Above 70°C, gluten coagulates when greater heat is applied. At this temperature, gluten release some moisture, which helps the starch hydrate and gelatinize.

At room temperature, some moisture will condense on the dough pieces as they enter the oven. This helps to maintain the dough's surface moisture while also helping to raise the dough's temperature since the condensation releases latent heat. The initial zone(s) of the oven must be kept humid, and in some situations, adding steam to the baking chamber has advantages as well. We have seen changes during baking that are mostly time- and temperature-dependent take place at various stages. They might cross paths and interact as shown in given *Figure 2.2*. (Davidson, I., 2016)

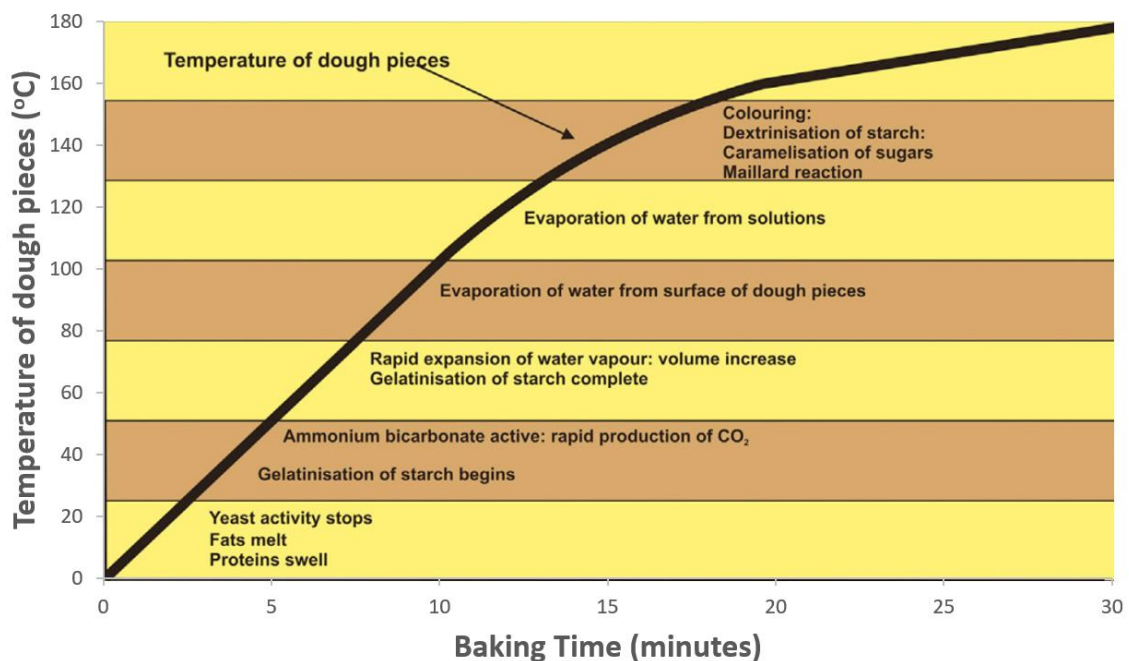


Figure 2.2: Temperature change of biscuits/cookies with respect to time (Davidson, I., 2016)

Moisture Removal

Low mixture content improves cookie given quality. The equal distribution of moisture from the centre to the exterior of the cookie prevents shattering during packing. As a result, sufficient heat and time are required for baking.

With parallel moisture removal, the volume of the dough expands from 3% at 50°C to 50% at 90°C. The dough material should remain wet so that optimum volume could be achieved. When the structure of biscuit settled up, evaporation of moisture takes place from dough surface at temperature around 100°C to 130°C and 2.5 to 3 % moisture content would be there in final product. (Davidson, n.d.)

Colour

Browning or colouring of biscuits/cookies is done by 3 processes as follows:

- i. Caramelisation
- ii. Dextrinization
- iii. Maillard reaction

High temperature is required for above browning processes and eventually appear when surface of biscuit/cookies is dry. During the last step of baking, the colouring is done.

2.1.2 Heat Transfer

There are 3 ways to transmit heat: conduction, convection, and radiation. When baking biscuits, all three heat transfer mechanisms are active. They vary in significance and impact on the final result, though, and how they are used depends on the oven's design.

Radiation

For baking biscuits, radiation is the primary means of heat transmission. The main sources are the heated surfaces of the baking chamber and the tubes or ducts that carry hot gases from the burners.. This radiant heat is effective and penetrating, and it doesn't cause any unfavourable side effects like quick drying or peeling of the dough pieces' surfaces.

We have noticed that a number of things influence the radiation, or transmission of thermal energy:

- i. The radiating surface's characteristics and emissivity as a result (how near to a "black body" it is).
- ii. The thermal energy that is delivered is inversely related to the square of how far apart the dough pieces are from the radiating surface. Heat transmission to the dough parts rises dramatically with a little decrease in distance.

$$\text{Intensity} = I/d^2$$

- iii. The difference in temperature between the dough pieces and the radiating surface. Heat transmission increases dramatically with a little rise in the radiating surface's temperature. The heat transmission is inversely correlated with the radiating surface's temperature to the power of 4.

Conduction

1. **Baking:** Conduction helps in transferring heat to the dough piece from oven. Transfer heat is affected by heat mass and temperature of the oven along with the band surface which is in contact with dough piece. When baking crackers, ovens with band preheat are very useful because they can immediately transmit heat into the base of the dough pieces. Using steel bands to bake soft doughs requires good conductivity.
2. **Oven Insulation:** The outer coverings of the ovens carry heat from the baking chamber, which adds to the heat loss to the bakery. To lessen loss of heat, Low thermal cond. Insulating material can be used.

Mineral wool is one material with a low heat conductivity that is frequently used for oven insulation. Molten rock, slag, glass, or stone is used to make mineral wool, which is then spun into fibres. Thermal conductivity of mineral wool - 0.06–0.10W/(mK) at baking temperatures (Figure 2.3) (Davidson, I., 2016)

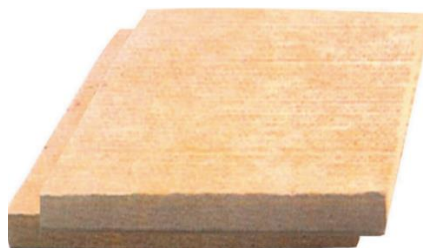


Figure 2.3 Mineral wool insulation for oven insulation (Davidson, I., 2016)

Convection

Hot air jets are used in convection baking, and they immediately impact the top of dough pieces and the bottom of the oven band. The dough pieces surfaces are effectively dried and coloured using this procedure.

Warmer air will go up due to rise in temperature by convective process.

Oven makers choose convection baking because it is very inexpensive to construct and has a fairly straightforward control system. The majority of convection ovens include a circulating fan with a speed remain constant and straightforward dampers to change the amount from upside to downside airflow.

(Figure 2.4) (Davidson, I., 2016)

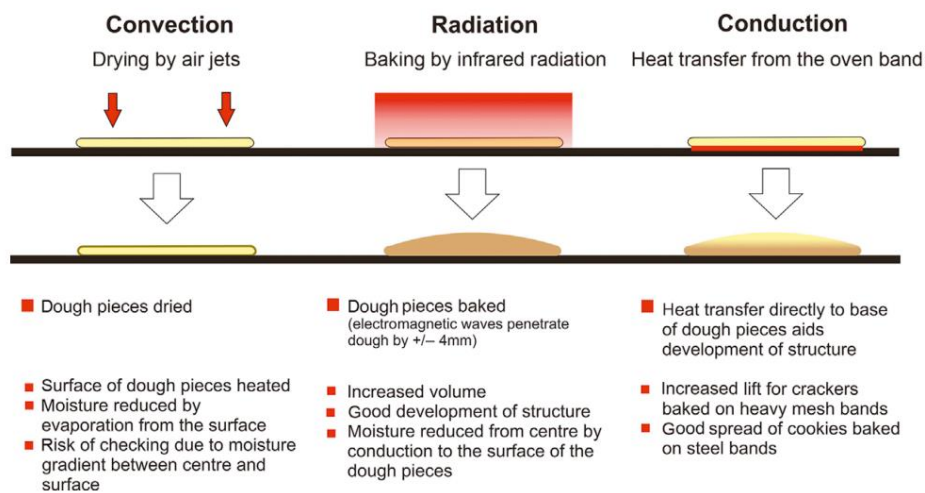


Figure 2.4: Summary of the effects of the modes of heat transfer (Davidson, I., 2016)

2.2 Review of receiver design

2.2.1 Scheffler dish-based bakery oven

Baking is a unit process that uses a lot of energy. By removing the realities of interrupted supply and fluctuating costs of non-renewable energy sources, the thermal application of solar energy is gaining interest in food operations. This research was done in order to design and develop a solar bakery unit as shown in Figure 2.5(Ayub et al., 2018b). It consists of a 10 m² Scheffler reflector that concentrates all beam radiations onto a secondary reflector, which further concentrates the beam radiations toward the solar bakery unit's heat receiver to heat the air circulated through the baking chamber using a

photovoltaic-powered fan. The design for even air distribution in the baking chamber was examined using a three-dimensional (3D) simulation that was CFD-based. The airflow distribution was pretty successful using the system configurations. The temperature at the receiver reached between 300 and 400°C, while the temperature at the entrance of the baking chamber was between 200°C and 230°C, which was enough to bake the majority of the items. The greatest amount of solar power at the receiver, with an average efficiency of 63 percent, was determined to be 3.46 kW. For a series of studies involving the baking of cakes, the total amount of energy available in the baking chamber was roughly 3.29 kW, and the energy needed to bake the cake was 0.201 kW. The energy usage ratio was determined to be 45 percent on average.

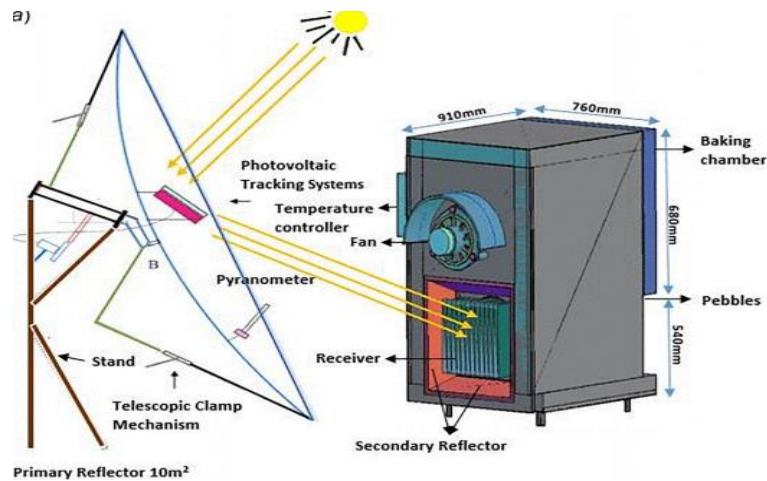


Figure 2.5: Scheffler Dish based solar oven(Ayub et al., 2018b)

2.2.2 Solar Fire Lytfire 5

A professional solar oven called the Lytfire 5 is designed for high temperature tasks like roasting and baking. The oven's maximum operational temperature is 300°C, and it has a 3.5 kW thermal power output. The footprint size of the entire tracking setup is 6 x 9 m, and the mirror area of the collector is approximately 5 m². In Figure 2.6, the breakdown of the Lytfire solar oven is displayed(Lytfire, 2022). According to the makers, they can produce 24 kg of bread every batch and 5 to 8 batches daily, depending on seasonal changes. It must be manually tracked by rotating the whole system for solar azimuth angles and inclining the mirrors for solar zenith angles. To guarantee that the focus remains on the concentrator receiver, this tracking must be performed every 10 minutes. Thermometers that are included with the oven may also provide temperatures automatically to a mobile app through Bluetooth.



Figure 2.6: Solar Fire Lytefire5 solar oven setup(Lytfire, 2022)

2.3 System Losses

In addition to producing biscuits of the finest quality, we also strive to provide baked goods at the lowest possible cost per kg. Therefore, we must take into account how much energy the oven uses. The efficiency of the oven is becoming increasingly important as energy costs rise in practically every nation. In other nations, like India, fuel is quite costly and makes up a significant portion of the overall cost of manufacturing.

The energy needed to heat the oven is largely utilised to bake the biscuit, create the desired structure, evaporate moisture from the dough, and colour the finished product. Each variety of biscuit needs a specific quantity of energy to produce a product of high quality.

Energy is wasted in a number of ways along with the energy necessary to bake a quality product (Davidson, n.d.,2016)

- i. By removing humid air from each oven zone
- ii. By loss of heat through the outer part and insulation of oven
- iii. By hot air leakage from oven delivery end
- iv. Heat loss during in-out of baking product

2.4 Energy and Mass balance in baking chamber

2.4.1 Thermal analysis of baking process

Due to heat and mass transmission mechanisms, the drying air conditions vary continually throughout baking. For the full thermal study, the heating and humidification processes were specified. Solar bakery unit for thermal study is shown in *Figure 2.7* (Ayub et al., 2018a). Different locations are:

- i. Inlet air for the receiver
- ii. Hot air from zigzag receiver
- iii. Hot air entering the baking chamber
- iv. Outflow air
- v. Recycled air after passing through pebble bed

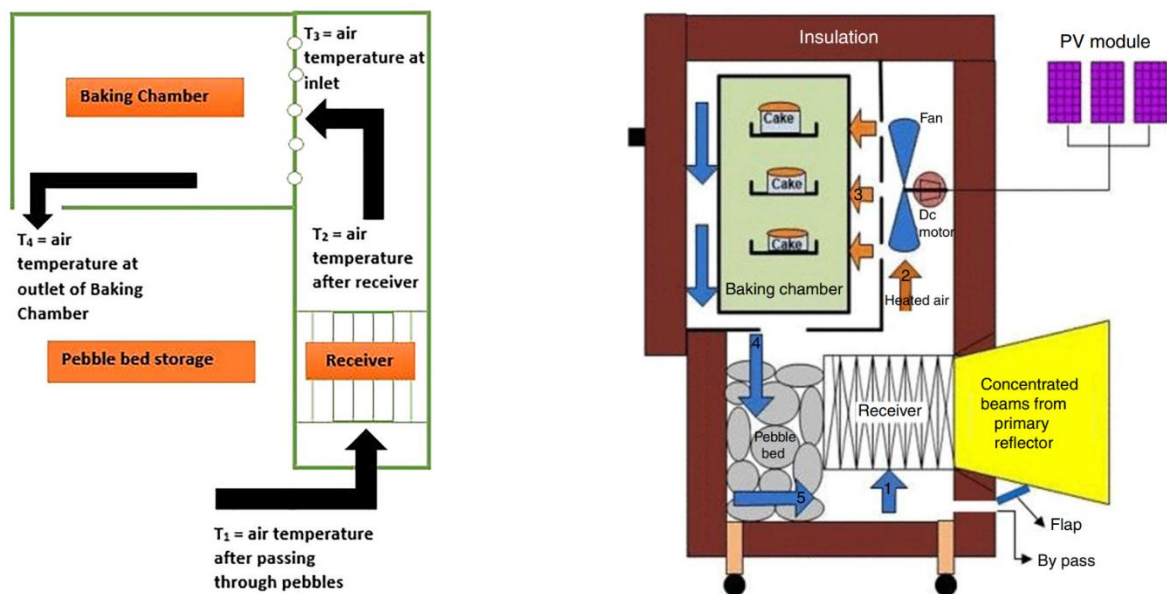


Figure 2.7: Schematic illustrating the progression of air quality at different locations within the solar bakery unit during the baking process. (Ayub et al., 2018a)

Receiver efficiency is given by:

$$\eta_r = \frac{Q_d}{Q_r} \quad 2.1$$

$$Q_d = mC_p(T_2 - T_1) \quad 2.2$$

$$Q_r = \frac{A_p \cdot I_b}{1000} \quad 2.3$$

The aperture area was calculated using the following equation 2.4

$$A_p = A_c \cos(43.23 \pm \delta/2) \quad 2.4$$

Considering the baking chamber as our system, a schematic for energy and mass balance analysis is shown in *Figure 2.8* (Ayub et al., 2018a). Let us take air properties at the inlet air as (m_i, w_i, T_i) and outlet air as (m_o, w_o, T_o) , where m is air mass flow rate, w is air relative humidity, T is air temperature and subscript i is used for inlet and o for outlet. Q amount of heat is required for cooking which we calculated above.

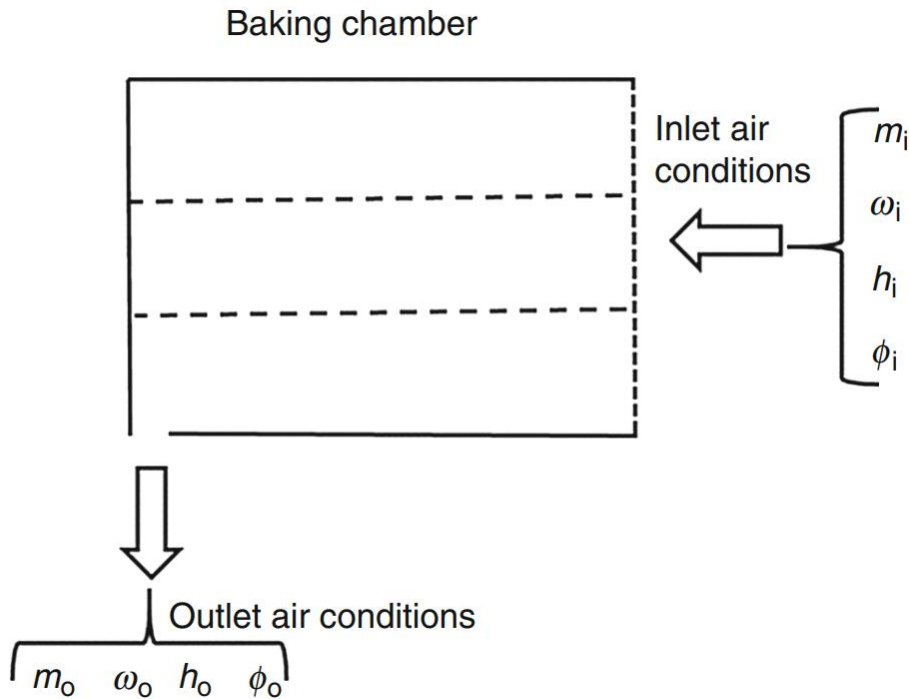


Figure 2.8: Inlet and outlet conditions of air in baking chamber (Ayub et al., 2018a)

2.4.2 Mass Conservation

Heating Process

The relative humidity of the air fell and its energy rose as it moved through the receiver. The air mass balance over a receiver with a unit volume may be defined as the relative humidity of the air fell and its energy rose as it moved through the receiver. The air mass balance over a receiver with a unit volume may be defined as:

$$m_1 = m_2 \quad 2.5$$

The humidity will be the same since the air conditions at points 3 (the entrance of the baking chamber) and 2 (the outlet of the receiver) are same.

$$\omega_2 = \omega_3 \quad 2.6$$

Baking Process

While a very little quantity of moisture was present in the inflow air, moisture is mixed with the drying air throughout the baking process. As a result, the air leaving the baking chamber will have a water content that may be expressed as

$$m_{bco} \omega_{bco} = m_{bci} \omega_{bci} + m_{bcinside} \omega_{bcinside} \quad 2.7$$

2.4.3 Energy balance

Heating process

The bakery component, receiver is responsible for imparting energy into coming air. The energy balance equation across the receiver can be written as

$$Q_{1-2} \text{ or } Q_{\text{net available}} = m_2 h_2 - m_1 h_1 \text{ or } m_{ro} h_{ro} - m_{ri} h_{ri} \quad 2.8$$

It is also possible to determine the quantity of energy that was transmitted to the air while passing by the receiver as

$$Q_{1-2} = mc_p(T_2 - T_1) \quad 2.9$$

Baking Process

It is challenging to utilise the baking of air potential throughout the baking process. The unused energy at the output is therefore often directed to recirculate and is stated as

$$Q_{wasted/recirculated} (m_4 h_4) = Q_{net\ available} - Q_{Energy\ utilized} \quad 2.10$$

In order to store heat, the energy is stored in the pebble bed near the outlet.

The formula for the amount of energy used in the baking chamber is

$$Q_{3-4} = mc_p(T_3 - T_4) \quad 2.11$$

Energy utilization ratio (EUR) of the baking chamber is given as

$$EUR = \frac{heat\ utilised}{heat\ supplied} = \frac{(c_{p_i} T_i - c_{p_o} T_o)}{(c_{p_i} T_i - c_{p_a} T_a)} \quad 2.12$$

2.5 Set-up of previous experiment

The collector is based on novel Fresnel Reflector concentrated thermal technology. It comprises of a 48 number of flat rectangular mirrors of dimension 52 cm x 15 cm are to place on the collector with 3 rows of 16 mirrors each. The construction of the setup is shown in Figure 2.9. Each of these rows can be individually rotated to adjust to sun's zenith angle while the entire setup can be moved about the central pivot point to adjust for the solar azimuth angle. As of the current prototype both these tracking movements are kept for manual control but could be modified later to better suit the application. The front glass covering the side of receiver that faces the concentrated solar radiation experienced a unequal thermal expansion to the nature of the solar image formed. This led to cracking and breaking of the mirror. To tackle this problem the glass was cut into three vertical pieces and then fit so that uneven expansion would not cause any stress and breaking. While operating the tracking for azimuthal angle needed to be done at-least every 10 min while that for zenith angle needed to be done at-least every 30 min.



Figure 2.9: Actual Setup in field testing (Jagtap, Kedare and Modi, 2021)

2.6 Experimentally achieved results

Cookies have been the target bakery product and thus different batch sizes have been tried. Typical internal temperature of the cookie followed a pattern like that shown in the following Figure 2.10 (Jagtap, Kedare and Modi, 2022)

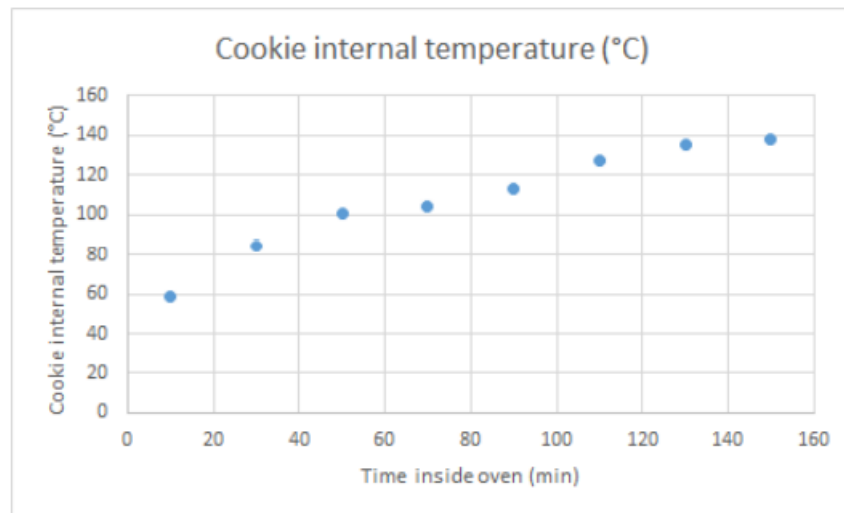


Figure 2.10: Temperature rise profile inside cookies (Jagtap, Kedare and Modi, 2022)

The graph has been plotted for 3.4 kg dry weight cookie batch and thus the trend to be observed should be independent of time scale, though it has been plotted for the sake of completeness. One can observe that the temperature inside cookie rises gradually till it nears boiling point, i.e 100°C. The curve becomes slightly flat at this instance and then increment starts again. In literature the Browning reaction (Milliard reaction) that is said to give bakery products its aroma and color is said to happen at temperature (oven temperature) of above 150°C and continues in the high temperature zone till 180-190°C.

Now, the time taken for baking has been plotted against the dry weight of resultant final product in *Figure 2.11* (Jagtap, Kedare and Modi, 2022). The average power entering the oven chamber in terms of optical flux during the tests was not constant across different loading conditions has to be noted. The energy consumption for baking also includes the energy absorbed by trays along with the cookies, as the trays were at ambient temperature while loading. Time requirement shows a minimum with for a dry output of 2.3 kg. But the power available for baking is different and thus cannot help in concluding as to which batch size is optimum.

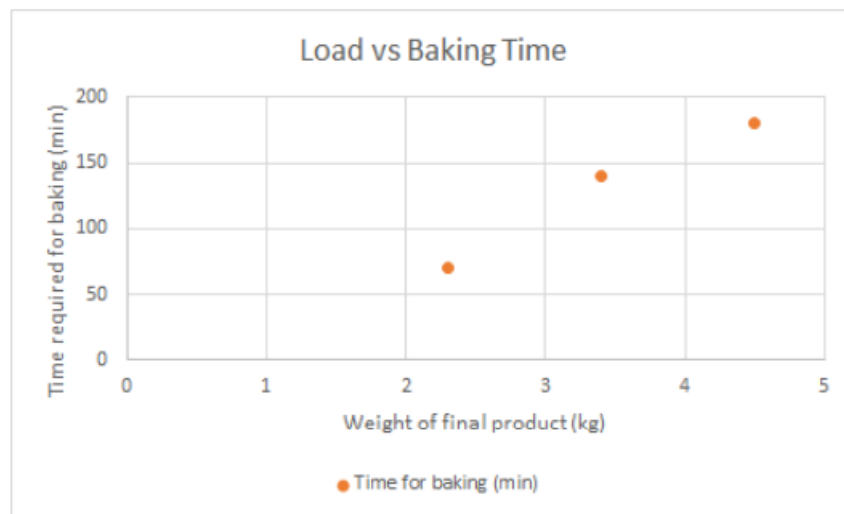


Figure 2.11: Average time consumption for different loads (Jagtap, Kedare and Modi, 2022)

The energy consumption per kg of cookies is seen to be fairly constant as shown in *Figure 2.12* (Jagtap, Kedare and Modi, 2022). Even so, out of the batches tried the smallest batch size of 2.3 kg is seen to show (marginal difference) lowest energy consumption per kg of cookies. The average value of energy consumption being 1330 kJ per kg of cookies. The calculations for 5 kg batch (against initially estimated) needed modification, as the weight of the trays was overestimated, and the final temperature of cookies was also different. The formulation used in design process when modified gives a power consumption of 1000 kJ/kg of dry cookies. Thus, the estimated power consumption is 24% lower than actual energy consumption. Another failed test where around 7.5 kg of wet cookies were tried failed after performing the test for about 4 hrs as the cookies remained wet and unbaked. This could be owing the fact that in the working hours of bakery a total of 7.5 kg wet weight is not manageable and added to that is the moisture removal ability of the oven, where the air saturation could be reached at such a high

load. Thus, smaller batch sizes such as 2.5 kg or 3.5 kg should be preferred over larger batch sizes. Since the batch size is not affecting the energy consumption, on a safer side to save wastage of food material smaller batches could be preferred. While on bright days slightly larger batches like 4.5-5 kg could also be baked.

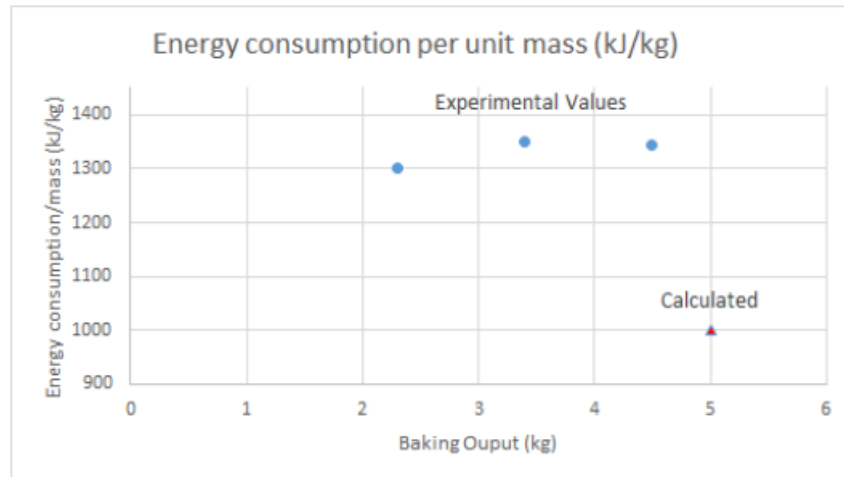


Figure 2.12: Energy consumption per kg for different loads (Jagtap, Kedare and Modi, 2022)

This chapter provides an overview of the literature review conducted for this study. It covers various aspects, including the baking process, a review of different receiver designs, an examination of system losses, and an analysis of energy and mass balance within the baking chamber.

Chapter 3

Development of Methodologies

3.1 View Factor Calculation using Steady-State Thermal Analysis in ANSYS:

3.1.1 Introduction:

View factor calculation is an important aspect of steady-state thermal analysis in engineering applications. It is an important parameter required to obtain radiation losses from surfaces. ANSYS, a widely used simulation software, provides powerful capabilities for calculating view factors between surfaces within a given domain. This presents the procedure to calculate view factors using steady-state thermal analysis in ANSYS.

3.1.2 Methodology:

The calculation of view factors using steady-state thermal analysis in ANSYS involves the following steps:

Step 1: Geometry setup:

Created a three-dimensional (3D) model of the Receiver domain in ANSYS Design Modeler. Ensured that the geometry accurately represents the surfaces for which the view factors are to be calculated.

There are 3 surfaces mentioned in the solar receiver for getting radiation value. Surface 1 is the walls of the receiver i.e., top wall, bottom wall, right wall, left wall, and back side cylindrical portion as shown in the *Figure 3.1*. Surface 2 is tray and cookies as shown in the *Figure 3.2*. Surface 3 is a radiation wall as shown in the *Figure 3.3*.

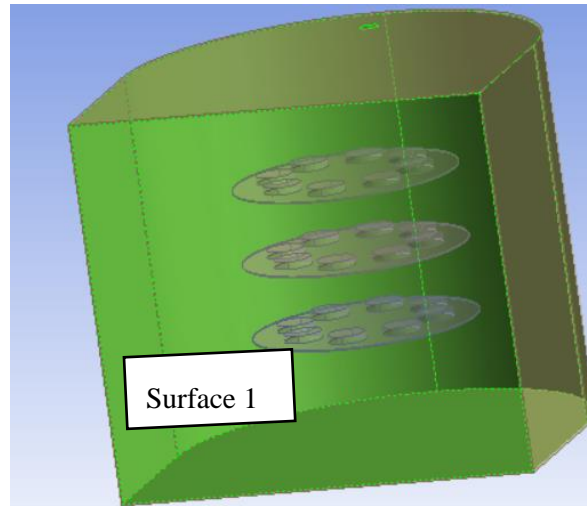


Figure 3.1: Surface 1 is considered in calculating view factors i.e., top wall, bottom wall, right wall, left wall, and back side cylindrical portion

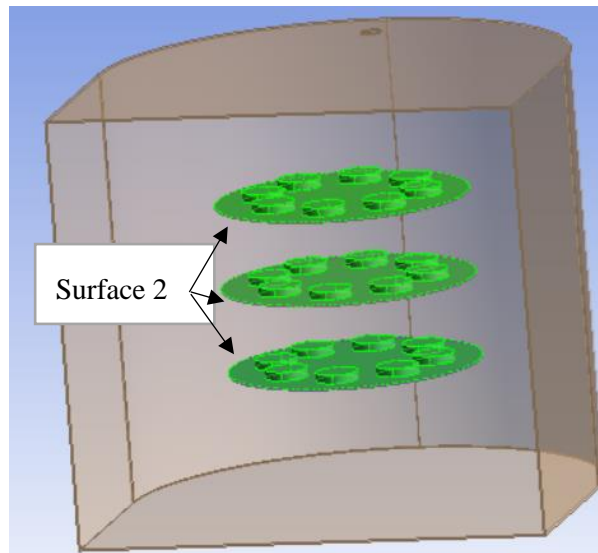


Figure 3.2: Surface 2 is considered in calculating view factors i.e., Trays and cookies

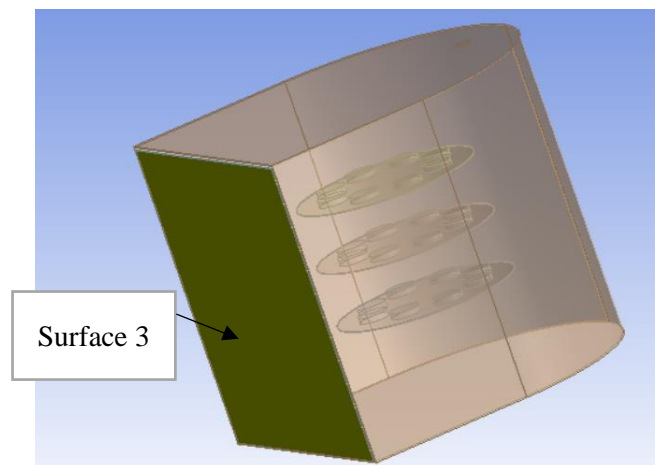


Figure 3.3: Surface 3 is considered in calculating view factors i.e., Radiation wall

Step 2: Meshing

Generated a high-quality mesh for the receiver domain using the Meshing module in ANSYS as shown in *Figure 3.4*. The mesh has sufficient resolution to capture the surface details and accurately computed the view factors. Used appropriate meshing techniques based on the geometry and analysis requirements. The number of nodes is 19174 and number of elements are 8658.

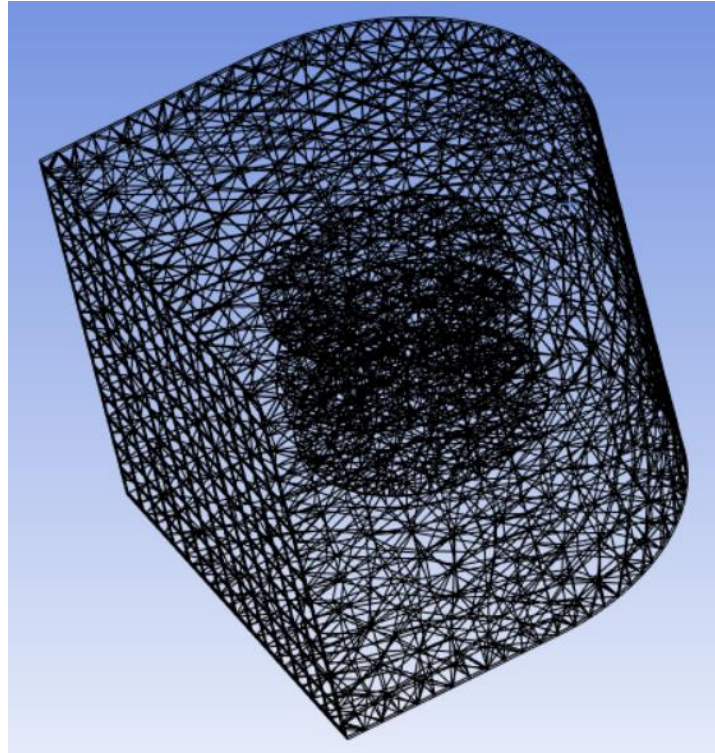


Figure 3.4: Meshing of Receiver

Step 3: Material Assignment

Steel has been used for receiver walls and trays. Glass has been used for radiation walls. It is important to note down that the View factor is independent of the material used for interacting surfaces. However, it depends on the following factors:

- i. Geometry: The geometry of the surfaces involved plays a crucial role in determining the view factors. The shape, size, orientation, and proximity of the surfaces affect the view factor values. Complex geometries may require additional considerations, such as surface splitting or mesh refinement, to accurately calculate the view factors.

- ii. **Surface Properties:** The thermal properties of the surfaces, such as emissivity and reflectivity, influence the view factor values. Surfaces with higher emissivity tend to exchange more thermal radiation with their surroundings, resulting in higher view factors.
- iii. **Temperature:** The temperature of the surfaces affects the view factor calculation, especially in thermal radiation analysis. The temperature difference between surfaces can significantly impact the amount of radiation exchanged and, consequently, the view factors.
- iv. **Medium Properties:** The properties of the medium between the surfaces, such as its thermal conductivity and refractive index, can affect the view factors. For example, in radiation analysis, the presence of a medium with high absorption or scattering properties can alter the view factor values.
- v. **Relative Position and Orientation:** The relative position and orientation of the surfaces influence the view factor calculation. Surfaces that face each other directly have a higher view factor compared to surfaces that are at oblique angles or partially obstructed.

Step 4: Boundary Conditions

It is an important step in simulation to define the boundary conditions for the thermal analysis.

Temperature and radiation heat flux boundary condition has been defined for all 3 surfaces such that a relatively higher temperature value is provided for that surface whose view factor is to be calculated with respect to other surfaces. This has to be done for all 3 surfaces. For simplification, the emissivity value is chosen to be 1 for all surfaces.

By changing temperature and emissivity values, small changes were noted in view factor values. Hence, below mentioned temperature and emissivity values give the approximate value of view factor.

Step 5: Solver setup

Solution settings have been configured for steady-state thermal analysis.

For the calculation of view factor of Surface 1 with respect to Surface 2 and Surface 3 i.e., F_{12} and F_{13} , temperature and emissivity values have been chosen as mention in Table 3.1

Table 3.1: Temperature input values of different surfaces to solver

	Surface 1	Surface 2	Surface 3
Temperature	150°C	22°C	22°C
Emissivity	1	1	1

For the calculation of view factor of Surface 2 with respect to Surface 1 and Surface 3 i.e., F_{21} and F_{23} , temperature and emissivity values have been chosen as follows:

	Surface 1	Surface 2	Surface 3
Temperature	22°C	150°C	22°C
Emissivity	1	1	1

For the calculation of view factor of Surface 3 with respect to Surface 1 and Surface 2 i.e., F_{31} and F_{32} , temperature and emissivity values have been chosen as follows:

	Surface 1	Surface 2	Surface 3
Temperature	22°C	22°C	150°C
Emissivity	1	1	1

Step 6: Calculation of view factors

Results obtained from ANSYS post-processing have been analysed to interpret the view factors.

The radiation probe provides different radiation values for different surfaces as mention in Table 3.2

Table 3.2: Radiation values at different surfaces

Surfaces	Outgoing net radiation (W)	Emitted radiation (W)	Reflected radiation (W)	Incident Radiation (W)
Surface 1 (150°C)	683	2354	1	1670
Surface 2 (22°C)	341	200	0.0002	541
Surface 3 (22°C)	336	121	0.0001	457
Surface 1 (22°C)	338	557	0.0006	895
Surface 2 (150°C)	395	844	0.4	448
Surface 3 (22°C)	53	121	0.0001	174
Surface 1 (22°C)	339	557	0.0006	896
Surface 2 (22°C)	53	200	0.0002	253
Surface 3 (150°C)	389	510	0.2	121

- $F_{12} = \frac{\text{Net radiation of surface 2}}{\text{Emitted radiation of surface 1}} = \frac{341}{2354} = 0.145$
- $F_{13} = \frac{\text{Net radiation of surface 3}}{\text{Emitted radiation of surface 1}} = \frac{336}{2354} = 0.143$
- $F_{11} = \frac{\text{Incident radiation of surface 1}}{\text{Emitted radiation of surface 1}} = \frac{1670}{2354} = 0.71$
- $F_{21} = \frac{\text{Net radiation of surface 1}}{\text{Emitted radiation of surface 2}} = \frac{338}{844} = 0.4$
- $F_{23} = \frac{\text{Net radiation of surface 3}}{\text{Emitted radiation of surface 2}} = \frac{53}{844} = 0.063$
- $F_{22} = \frac{\text{Incident radiation of surface 2}}{\text{Emitted radiation of surface 2}} = \frac{448}{844} = 0.531$
- $F_{31} = \frac{\text{Net radiation of surface 1}}{\text{Emitted radiation of surface 3}} = \frac{339}{510} = 0.665$
- $F_{32} = \frac{\text{Net radiation of surface 2}}{\text{Emitted radiation of surface 3}} = \frac{53}{510} = 0.104$
- $F_{33} = \frac{\text{Incident radiation of surface 3}}{\text{Emitted radiation of surface 3}} = \frac{121}{510} = 0.238$

3.2 Ray Independence Test using COMSOL

A separate investigation was conducted to determine the number of ray intersections required for ray independence. Ray tracing is a technique for rendering images by tracing the path of light rays from a light source to a camera. Ray independence is a property of a ray tracing algorithm that ensures that the results of the algorithm are not sensitive to the number of ray intersections.

To determine the number of ray intersections required for ray independence, we can use the following steps:

- i. Create a simulation model of the scene we want to render.
- ii. Set up the simulation to use ray tracing.
- iii. Run the simulation for a small number of ray intersections.
- iv. Compare the results of the simulation with the known results of the scene.
- v. Increase the number of ray intersections and repeat steps 3 and 4.
- vi. Continue increasing the number of ray intersections until the results of the simulation do not change significantly.

The number of ray intersections required for ray independence will depend on the complexity of the scene and the accuracy required. For simple scenes, a small number of ray intersections may be sufficient. For complex scenes or scenes where high accuracy is required, a large number of ray intersections may be required.

Ray independence is an important property of ray tracing algorithms because it ensures that the results of the algorithm are accurate and reliable. By determining the number of ray intersections required for ray independence, we can ensure that our ray tracing simulations are accurate and reliable.

Mirror size plays an important role in proper functioning of reflector surface. Smaller the mirror size better will be the concentration due to better fitting into the reflector profile curvature. Very small mirror size will have feasibility issues such as increased fabrication time and fixation issues. Thus, there is a need to choose the mirror size and arranging them in an array so that profile curvature is optimally utilized. Some gap is required between the adjacent mirrors: (a) to allow wind to pass through without

damaging the structure and (b) to allow shrinkage or expansion during seasonal adjustment using telescopic clamps.

3.2.1 Collector design

Description of collector:

The collector comprises of a number of flat rectangular mirrors arranged in three arrays on a frame as shown in *Figure 3.5*. The base of the collector frame is located at a distance X_{base} along the positive side of the x-axis and at a distance of Z_{base} from the xy plane. The collector frame is inclined to the x-axis at an angle β , which will be called as frame inclination angle. Mirrors are supported on carrier rods and these carrier rods would be free to rotate in the frame about their axis. The mirrors are not directly placed on the carrier rods but rather are supported using some supporting arm that gives a offset from the rods. The frame inclination β can be changed as there would be a hinge provided at the base of the frame. The collector is placed symmetrically about the xz plane facing the receiver which lies in the yz plane. The whole setup would be rotated so that the x-axis of the Global Coordinate System gets aligned along the direction of the solar azimuth angle effectively allowing solar rays to fall only in planes parallel to yz plane.

Collector's optical analysis:

The Collector design would mean setting up the positions of mirrors in the arrays and giving them appropriate inclinations so that the reflection of solar radiation falls at desired location i.e. at the receiver. These inclinations would be decided based on a design solar zenith angle θ_z and design frame inclination. Once these inclinations are determined the inclinations would get fixed. To cater for the changing solar zenith angles the collector would have two possible adjustments: the carrier rods could be rotated and the frame inclination could also be changed. The image spread and power collected for zenith angles other than the design zenith angles would be compared for different design positions. As a measure of image spread would be power received on the receiver surface.

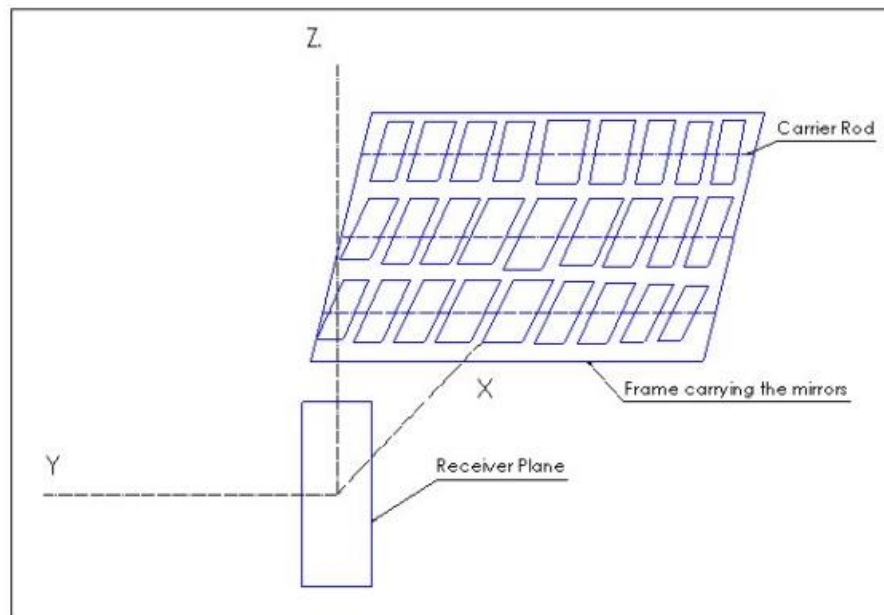


Figure 3.5: Collector placed in the Global Coordinate System

3.2.2 Prototype development using COMSOL:

Each mirror has a dimension of $52 \text{ cm} \times 15 \text{ cm}$ and 48 such are to be placed on the collector with 3 rows of 16 mirrors each with total mirror area of 3.7 m^2 . The dimensions data of each mirror in form of (x,y,z) is obtained using experimental set-up. The receiver is placed at origin of global coordinate system. This data is then arranged in specific form having (x,y,z) value of each mirror one by one is fed into COMSOL and is obtained.

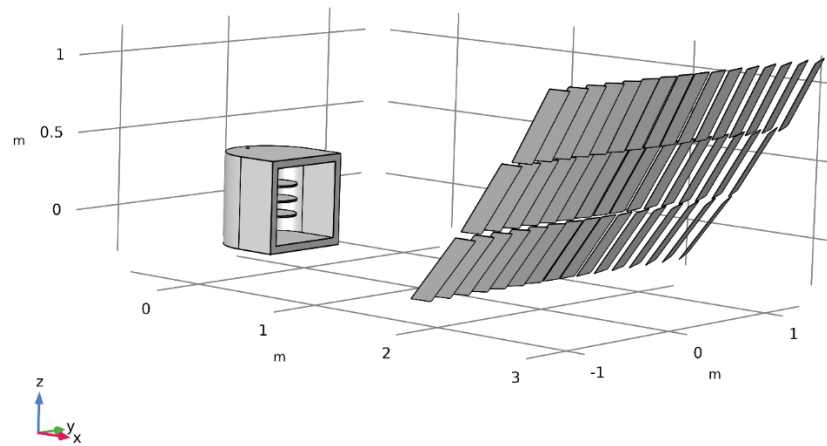


Figure 3.6: CAD model of receiver of Receiver and collector

3.2.3 Results:

Different number of incident rays have been studied. Table: shows the percentage of energy falling on different surfaces of receiver like tray 1, tray 2, tray 3 and cavity wall. The result shows that percent energy falling value does not change much from 10^5 to 10^6 number of rays.

Table 3.3: Percentage of energy falling for different number of rays

No. of rays	Cavity wall (%)	Tray 1 (%)	Tray 2 (%)	Tray 3 (%)	Total Receiver (%)
1000	69.3	9.7	10.4	10.6	100
10000	70.6	8.8	9.9	10.7	100
1.00E+05	70.2	8.9	10.1	10.7	100
1.00E+06	70.2	8.9	10.1	10.7	100

3.3 Losses In Receiver

3.3.1 Radiation Loss Calculations:

Radiative losses in a solar receiver occur when the receiver emits thermal radiation, resulting in the loss of heat energy. These losses can be significant, especially in high-temperature solar receivers. Here are some factors that contribute to radiative losses:

- 1. Emissivity of Receiver Surface:** The emissivity of the receiver surface determines how effectively it radiates thermal energy. A higher emissivity value indicates a greater tendency to emit radiation. For efficient operation, solar receivers typically use materials with low emissivity to minimize radiative losses.
- 2. Temperature Differential:** Radiative losses increase with the temperature differential between the receiver surface and its surroundings. The Stefan-Boltzmann law states that the rate of radiative heat loss is proportional to the fourth power of the temperature difference. Therefore, minimizing temperature differentials can help reduce radiative losses.
- 3. Surface Area and Geometry:** The surface area and geometry of the receiver can influence radiative losses. A larger surface area or complex shapes can increase the radiative heat transfer area, resulting in higher losses. Designing the receiver with compact and optimized geometries can help minimize radiative losses.
- 4. Enclosure Design:** The design of the receiver enclosure plays a role in radiative losses. If the enclosure has openings or gaps that expose the receiver to the surroundings, it can increase radiative heat losses. Proper insulation and sealing are necessary to reduce such losses.
- 5. Operating Environment:** The operating environment around the solar receiver affects radiative losses. If the receiver is exposed to low-temperature surroundings or to a cooler ambient atmosphere, radiative losses will be higher. Minimizing exposure to cooler environments and using insulation can help mitigate these losses.

To minimize radiative losses in a solar receiver, several strategies can be employed:

- a. Using materials with low emissivity coatings or surfaces that reflect thermal radiation back to the receiver can reduce radiative losses.
- b. Employing insulation materials with low thermal emissivity can limit heat radiation to the surroundings.
- c. Optimizing the receiver design to reduce surface area and intricate geometries can minimize radiative heat transfer.
- d. Utilizing selective coatings on the receiver surface can enhance solar absorption while reducing thermal radiation losses.
- e. Implementing proper enclosure design with insulation and sealing techniques can minimize exposure to low-temperature surroundings.

Radiation losses associated with the receiver for solar bakery:

There can be two types of radiative losses that can be occurred in the receiver for solar bakery:

1. Radiative loss from glass:

Radiative losses can occur from the glass mouth of a solar receiver due to the thermal radiation emitted by the receiver's hot surface. The glass mouth acts as a window through which thermal radiation can escape, resulting in energy losses. Here are some factors that influence radiative losses from the glass mouth of a solar receiver:

- **Emissivity of the Glass:** The emissivity of the glass material used for the receiver's mouth determines its ability to emit thermal radiation. Higher emissivity values indicate a greater tendency to emit radiation. To minimize radiative losses, it is beneficial to select glass materials with low emissivity, which will reduce the amount of energy radiated through the glass mouth. The emissivity value for glass used in experimental set-up is 0.9 (Jagtap, Kedare and Modi, 2022).
- **Temperature Differential:** Radiative losses increase with the temperature difference between the hot receiver surface and the glass mouth. According to the Stefan-Boltzmann

law, radiative heat loss is proportional to the fourth power of the temperature difference. Thus, minimizing the temperature differential can help reduce radiative losses.

- **Glass Thickness and Thermal Conductivity:** The thickness and thermal conductivity of the glass also affect radiative losses. Thicker glass tends to have higher thermal resistance, resulting in reduced heat transfer through conduction. However, thicker glass may increase radiative losses due to the larger surface area exposed to the surroundings. Selecting an optimal thickness and material with appropriate thermal conductivity can help minimize radiative losses.

2. Radiative loss from walls:

Radiative losses from the walls towards the glass in a solar receiver occur when thermal radiation emitted by the walls is absorbed or transmitted through the glass, resulting in energy losses. These losses can reduce the overall efficiency of the receiver. Here are some factors that influence radiative losses from the walls toward the glass in a solar receiver:

- **Emissivity of the Walls:** The emissivity of the walls surrounding the receiver determines their ability to emit thermal radiation. Higher emissivity values indicate a greater tendency to emit radiation. If the walls have high emissivity, they will emit more thermal radiation toward the glass, increasing radiative losses. To minimize these losses, it is beneficial to use wall materials with low emissivity.
- **Glass Transmittance:** The transmittance properties of the glass play a role in radiative losses. If the glass has a high transmittance for thermal radiation emitted by the walls, a larger amount of radiation will pass through the glass, resulting in increased energy losses. Using glass with low transmittance for thermal radiation can help reduce these losses.
- **Geometry and Orientation:** The geometry and orientation of the walls in relation to the glass can influence radiative losses. If the walls are located at angles that facilitate direct line-of-sight radiation toward the glass, the losses will be higher. Optimizing the geometry and orientation of the walls can help minimize radiative heat transfer toward the glass.

- **Wall Coatings and Treatments:** Applying coatings or treatments to the walls can modify their radiative properties and help reduce energy losses. For instance, using coatings with low emissivity or reflective properties can reduce the amount of radiation emitted towards the glass, thereby minimizing radiative losses.

To minimize radiative losses from the walls towards the glass in a solar receiver, it is important to select wall materials with low emissivity, reduce the temperature differential between the walls and the glass, and use glass with low transmittance for thermal radiation. Additionally, optimizing the geometry and orientation of the walls and applying coatings or treatments to the walls can help further reduce energy losses through radiative heat transfer toward the glass.

Calculation of radiative loss in the receiver at steady state for simple case:

In a basic scenario, we consider that the receiver wall at a temperature of 480K is surrounded by semi-cylindrical surfaces on the left, right, top, bottom, and back. These surfaces act as boundaries, and through convection, they transfer heat to the surrounding air. The heated air then further transfers heat to the glass, leading to an increase in its temperature. Radiation losses can be calculated as:

$$Q_R = [\sigma \varepsilon_1 F_{12} A_1 (T_w^4 - 300^4)]_{Wall} + [\sigma \varepsilon_2 F_{2a} A_2 (T_g^4 - 300^4)]_{Glass} \quad 3.1$$

Table 3.4: Values of variables used in equation 3.1

Variables	Walls	Glass
Emissivity	0.85	0.9
View Factor	0.22	1
Area(m ²)	1.299	0.2856
Surface Temp(K)	480	370
Ambient Temp(K)	300	300
Radiation Heat transfer (W)	619	155

3.3.2 Convective Loss:

The amount of convective loss is proportional to the difference between the receiver temperature and the temperature of the surrounding air. This means that a small increase in the receiver temperature can

lead to a significant increase in convective loss. The presence of any gaps or cracks in the receiver surface can also increase convective losses. These gaps and cracks can allow the surrounding air or water to come into contact with the receiver surface, which will increase the amount of heat that can be lost by convection. In experimental set-up convective loss can be expected more than numerical set-up because practically there are more gaps between different surfaces.

Convective losses associated with the receiver for solar bakery:

There are two types of convective losses that can be occurred in receiver for solar bakery:

1. Convective mass transfer:

This particular form of heat loss happens through an opening, specifically a pressure outlet located on the top wall of the receiver. As a result, air flows out through this opening, carrying away heat in the form of a heated mass.

2. Convective heat from outer surface of glass:

Convective heat transfer from the outer surface of the glass in a solar receiver occurs when there is a flow of fluid (ambient air) over the glass surface, resulting in the transfer of heat energy to the fluid and subsequent energy losses. The convective heat transfer from the glass surface can contribute to the overall heat losses of the system. Factors that influence convective heat losses from the glass surface include the velocity (in this case natural convection) and temperature of the fluid, the thermal conductivity of the glass, and the surface area and geometry of the glass. As the fluid moves over the glass surface, it absorbs heat from the glass through convection and carries it away, resulting in energy dissipation.

Calculation of convective loss in the receiver at steady state for simple case:

In a basic scenario, we consider that the receiver wall at a temperature of 480K is surrounded by semi-cylindrical surfaces on the left, right, top, bottom, and back. These surfaces act as boundaries, and through convection, they transfer heat to the surrounding air. The heated air then further transfers heat to the glass, leading to an increase in its temperature. Convective losses can be calculated as:

$$Q_c = [hA(T_{glass} - 300)]_{Outer\ Glass} + [mC_p(T_{air} - 300)]_{Convective\ mass\ transfer} \quad 3.2$$

Table 3.5: Values of variables used in equation 3.2

Variables	Glass	Convective mass transfer
Area(m ²)	0.2856	-
Surface Temp(K)	370	478
Ambient Temp(K)	300	300
Heat transfer coefficient (W/m ² K)	7.2	-
mass flow rate (g/s)	-	0.85
Cp value (J/g-K)	-	1
Convective Heat Transfer (W)	143	151

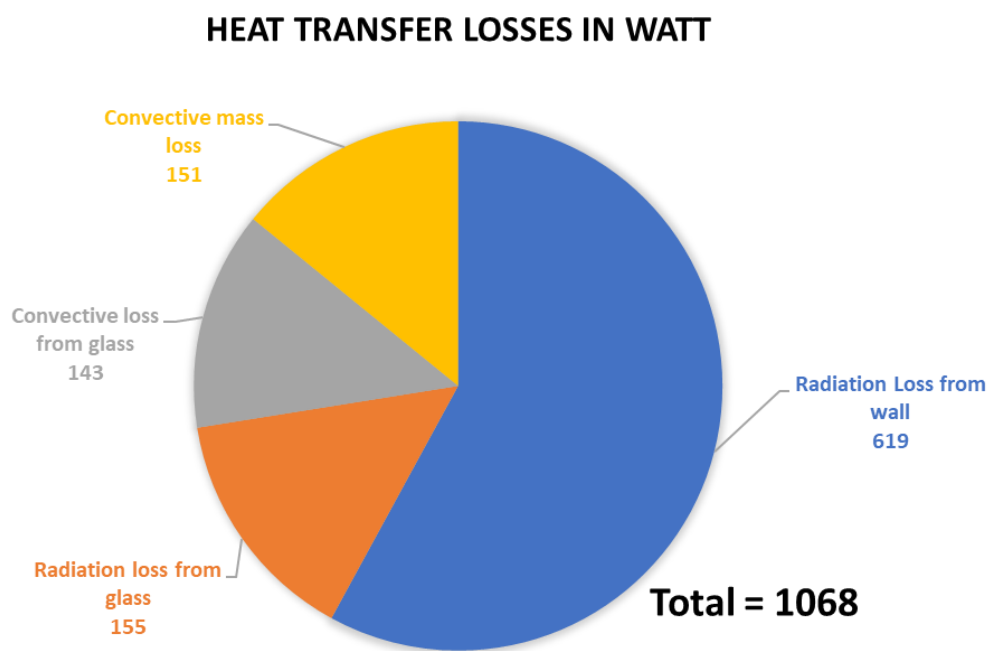


Figure 3.7: Share of radiative and convective heat transfer loss in receiver

3.4 Energy Balance equation of the receiver

The energy balance of a solar receiver is a fundamental concept that involves accounting for all the energy inputs and outputs within the receiver. It provides a comprehensive understanding of the energy flow and distribution within the system. In the context of a solar receiver for bakery applications, the energy balance involves considering various sources and sinks of energy.

The energy balance of a receiver is a calculation of the amount of energy that is absorbed by the receiver, the amount of energy that is lost through heat transfer, and the amount of energy that is transferred to the fluid flowing through the receiver. The energy balance can be expressed as follows:

$$Q_{inlet} = Q_{losses} + Q_{absorbed} \quad 3.3$$

$$Q_{inlet} = Q_{convection} + Q_{radiation} + Q_{absorbed} \quad 3.4$$

$$Q_{inlet} = I_{bn} \cdot A_{ap} \cdot \eta_{opt} \quad 3.5$$

$$= 750 \times 3.588 \times \cos 43.23 \times 0.51 \quad (\text{For } 750 \text{ W/m}^2 \text{ Solar irradiation})$$

$$= 1000 \text{ W}$$

$$Q_{convection} = [hA_2(T_{glass} - 300)]_{Outer\ Glass} + [mC_p(T_{air} - 300)]_{Convective\ mass\ transfer} \quad 3.6$$

$$Q_{radiation} = [\sigma \varepsilon_1 F_{12} A_1 (T_w^4 - 300^4)]_{Wall} + [\sigma \varepsilon_2 F_{2a} A_2 (T_g^4 - 300^4)]_{Glass} \quad 3.7$$

$$Q_{absorbed} = [m_{cookies} C_p \frac{\Delta T}{\Delta t}]_{cookies} + [m_{Wall} C_p \frac{\Delta T}{\Delta t}]_{Wall} + [m_{glass} C_p \frac{\Delta T}{\Delta t}]_{glass} \quad 3.8$$

3.5 Numerical Investigation:

The numerical analysis involved creating a three-dimensional model of the solar receiver using Ansys, considering the geometry, material properties, and boundary conditions. The receiver's geometry included intricate designs to maximize the absorption of solar energy and enhance heat transfer efficiency. Material properties such as thermal conductivity, specific heat capacity, and absorptivity were incorporated into the model to accurately simulate the energy transfer mechanisms within the receiver.

The simulation involved complex heat transfer and fluid flow phenomena, as the solar receiver was subjected to intense solar radiation and airflow. Ansys 2022 allowed to solve the governing equations for heat transfer using numerical methods, considering the solar input and convective heat loss. The simulation also accounted for any temperature-dependent properties of the materials used in the receiver.

3.5.1 Description of receiver geometry

The geometry of a solar receiver as shown in *Figure 3.8* for bakery applications is designed to maximize the absorption of solar energy. The receiver usually comprises a rectangular-shaped opening made of glass and a semi-cylindrical section made of steel material.

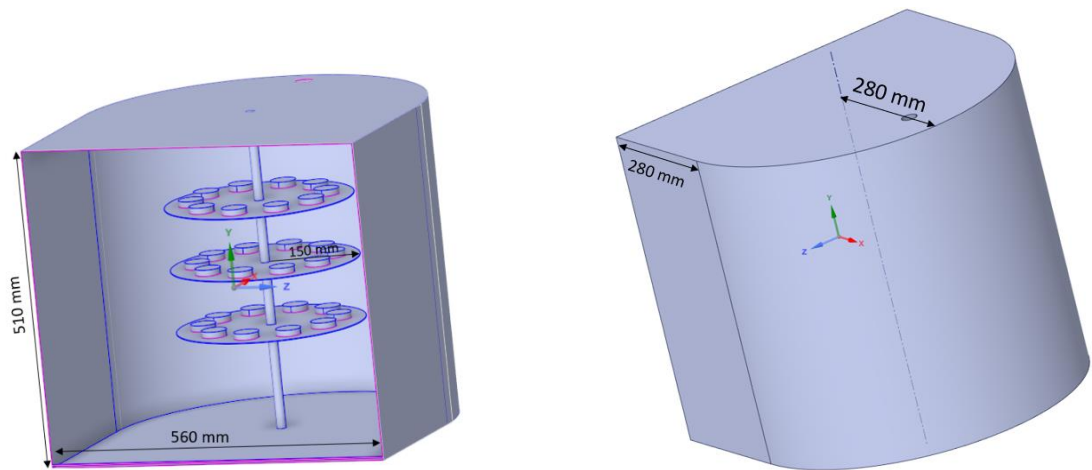


Figure 3.8: Receiver Geometry

There is total 3 trays and 30 cookies, 10 cookies per tray, have been considered. The trays are suspended from the rod. The dimensions used for model bakery receiver have referred from experimental set-up (Jagtap, Kedare and Modi, 2022) as shown in *Table 3.6* below.

Table 3.6: Geometrical Dimensions of Receiver

Surfaces	Dimensions (mm)
Width of Receiver Mouth	560
Height of Receiver Mouth	510
Length of Rectangular portion	280
Radius of Cylindrical portion	280
Thickness of wall	1
Diameter of Tray	300
Thickness of Tray	1
Diameter of cookie	75
Thickness of cookie	30
Diameter of rod	10
Length of rod	510
Diameter of hole	25

3.5.2 Meshing:

The meshing process is a critical step in the numerical analysis of a solar receiver for bakery applications using Ansys Fluent. In this report, we present a description of the meshing technique employed to accurately represent the receiver's geometry and facilitate accurate simulations of heat transfer and fluid flow phenomena.

To begin, the receiver's geometry, which consists of a rectangular mouth and semi-cylindrical walls structure with intricate internal trays and cookies, was imported into Ansys Fluent. The meshing process involved creating a high-quality computational mesh that captured the receiver's complex geometry while ensuring computational efficiency as shown in *Figure 3.9*.

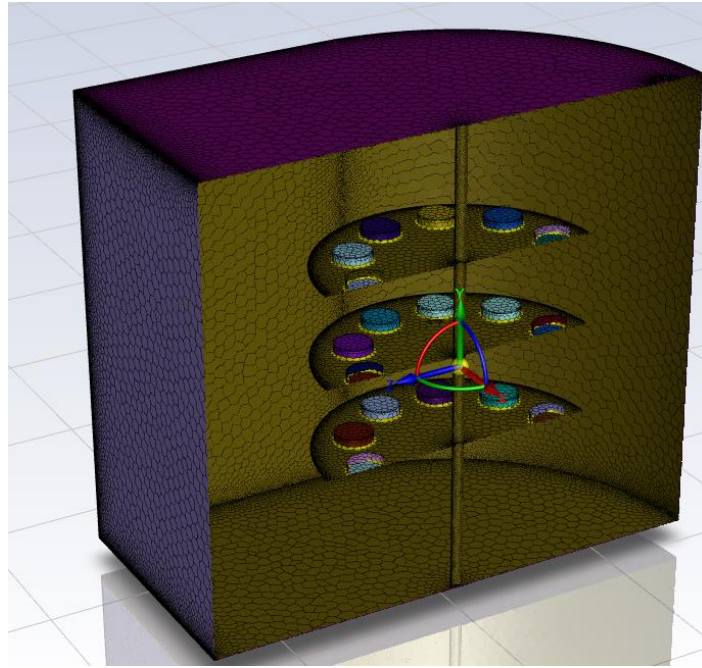


Figure 3.9: Meshing of receiver

The mesh density was carefully controlled, with finer mesh elements employed in regions of small size surfaces like cookie, hole, to capture the localized phenomena accurately. The quality of the generated mesh was assessed using various metrics, including mesh element aspect ratios, skewness, and expansion ratios. These metrics helped ensure the mesh's quality, minimizing numerical errors and maintaining computational stability during the simulations. The volume mesh has been filled with poly-hexacore mesh with size of 3.5 mm. Total number of cells are 5545517.

3.5.3 Grid dependency test

Table 3.7: Grid dependency test

Element size (mm)	Number of cells	Heat loss	Percentage change (%) w.r.t. its predecessor
8.8	1854666	174.1	-
7 (80%)	2190090	195	12
5.3 (60%)	2922904	215	10.25
3.5 (40%)	5545517	225.87	5.05
1.76 (20%)	30892906	228.72	1.26

3.5.4 Boundary Conditions

This presents a detailed description of the boundary conditions utilized to model the receiver's behaviour and evaluate its performance. The boundary conditions for the solar receiver for a bakery in ANSYS Fluent were set as follows:

1. The inlet and outlet boundary condition were set to a pressure of 1 atm and a temperature of 300 K. The walls of the receiver were set to a no-slip condition.
2. The solar radiation boundary condition (866W, 1000W, and 1133W) was applied to the mouth of the receiver constructed with glass material having thickness 4mm. The incident solar radiation intensity, direction, and spectral distribution were defined. The solar radiation was incorporated as a heat source term, accounting for the absorptivity of the receiver's surface. This boundary condition allowed for the accurate representation of the energy input from the sun and its impact on the receiver's temperature distribution.
3. The receiver's boundary is made of 1mm thick steel and is insulated to prevent heat loss.

The properties of material considered for receiver construction are mentioned in below *Table 3.8*.

Table 3.8: Material properties

Properties	Glass	Cookies	Steel
Density (kg/m ³)	2500	750	8030
Specific heat (J/kg K)	800	1500	502.48
Thermal Conductivity (W/m K)	0.8	0.5	16.27

3.5.5 Computational model:

To solve the governing equations for a solar receiver in a bakery using numerical methods, a computational model is employed. This model involves several key components and equations to simulate the heat transfer and fluid flow phenomena within the receiver. The following is a description of the computational model used to solve these equations. The CFD simulation is based on simultaneous solution of the system of equations describing the conservation of mass, momentum, and energy and these can be expressed as follows in equation 3.9, 3.10, and 3.11 (Kumara et al., 2019)

$$\nabla \vec{v} = 0 \quad 3.9$$

$$\rho \frac{D\vec{v}}{Dt} = \rho(\vec{g} - \nabla \vec{p} - \mu \nabla^2 \vec{v}) \quad 3.10$$

$$\rho C_p \frac{DT}{Dt} = k \nabla^2 T \quad 3.11$$

This chapter includes the methodology to achieve final results like calculation of losses and heat requirements, temperature variation at different surfaces in receiver, energy balance equation and numerical investigation.

Chapter 4

Results and Discussions

4.1 Numerical results:

The provided *Figure 4.1* displays the temperature distribution on various surfaces of the receiver after reaching a steady state with an input of 1000W solar radiation. It is evident from the figure that the temperature reaches its highest value at the back side of the wall. This can be attributed to the direct impact of solar radiation on the back side. On the other hand, the surfaces near the glass opening have comparatively lower temperatures. The air enters the receiver through a hole positioned beneath the glass opening, and its temperature at that location is approximately 300K, corresponding to atmospheric conditions.

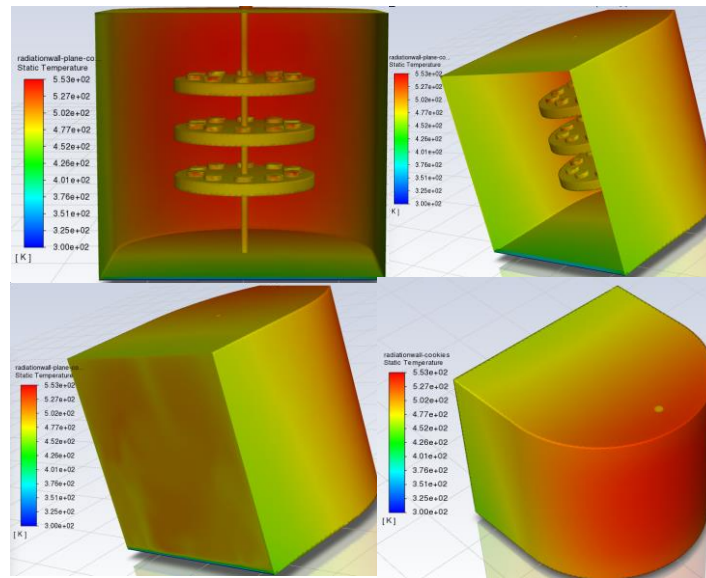


Figure 4.1: Temperature contours of receiver at input of 1000W

The temperature distribution inside the receiver is depicted in the *Figure 4.2* below, considering a mid-plane. The diagram shows cookies and air on the assumed plane. We can observe that hot air rises

upwards due to the thermosiphon effect, and this hot air also heats up the cookies. The cookies are additionally heated by radiation from the glass opening, heated trays, and walls. Initially, the cookies positioned in front of the glass opening are relatively hotter than those placed near the back side wall, as they receive direct radiation. However, at steady state, the temperature of all cookies becomes uniform.

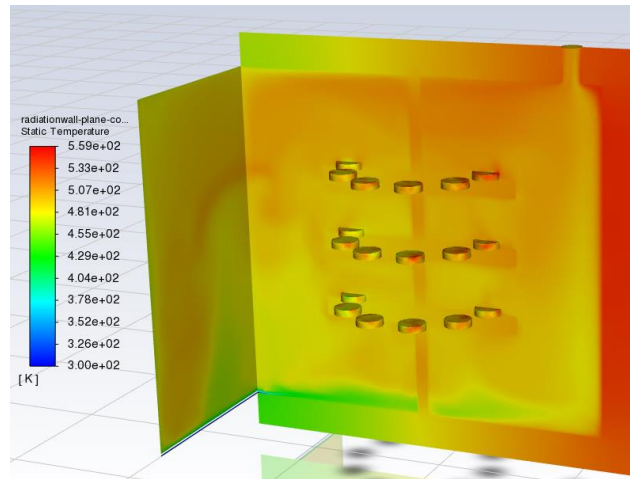


Figure 4.2: Temperature distribution inside receiver

4.2 Comparison of experimental and numerical results

4.2.1 Cookie temperature:

In this analysis, the temperature of the cookie was examined under varying heat inputs as shown in *Figure 4.3*. The findings demonstrate that the temperature variation of the cookie at an input of 1000W closely resembles the experimental results with deviation of less than 5% for the cookie temperature data. Additionally, the temperature of the cookie was plotted for different heat inputs (866 W, 1000 W, and 1133 W). It can be observed that as the heat input increases, the temperature of the cookie also rises, and the steady state is reached more quickly.

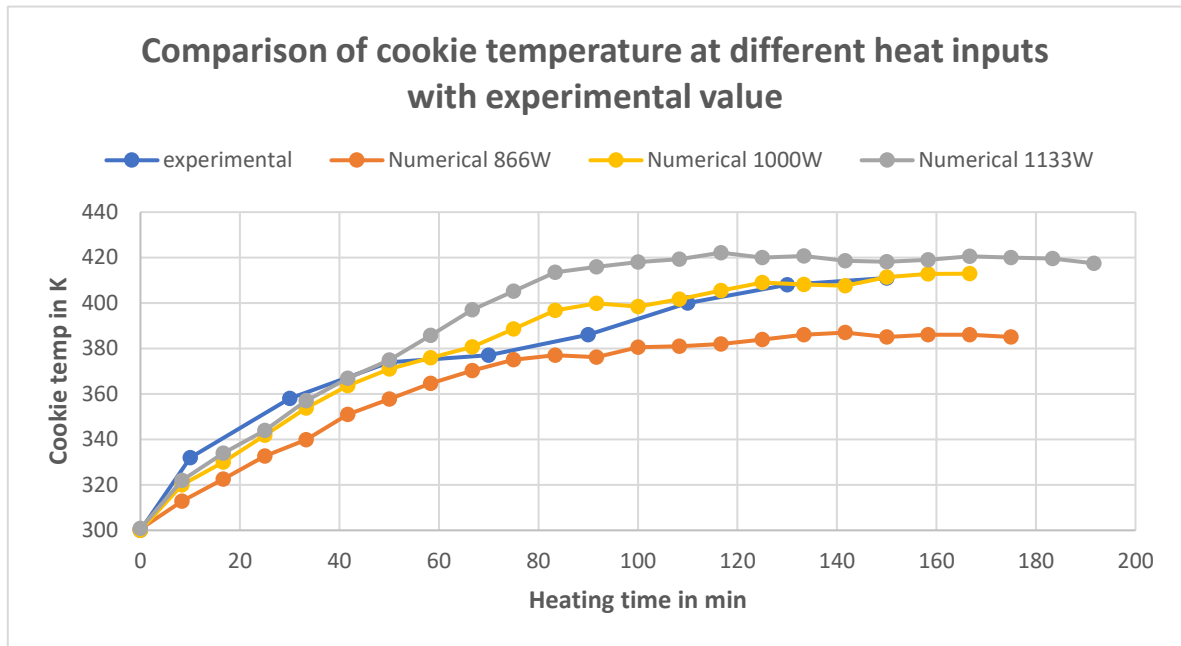


Figure 4.3: Comparison of cookie temperature at different heat inputs with experimental value

4.2.2 Wall temperature:

In this analysis, the temperature of the wall was investigated under different heat inputs as shown in *Figure 4.4*. The results reveal that the temperature variation of the wall closely resembles the experimental findings, similar to the temperature analysis of the cookies with deviation of less than 14% for the wall temperature data. Additionally, the temperature of the wall was plotted for various heat inputs (866 W, 1000 W, and 1133 W). It can be observed that as the heat input increases, the temperature of the wall also rises, and the steady state is attained more rapidly.

However, it should be noted that in the experimental results, a slight decrease in temperature occurs due to the loading process of cookies into the receiver, resulting in some heat loss. To replicate this situation in the simulation, the radiation input can be temporarily removed during that specific time interval.

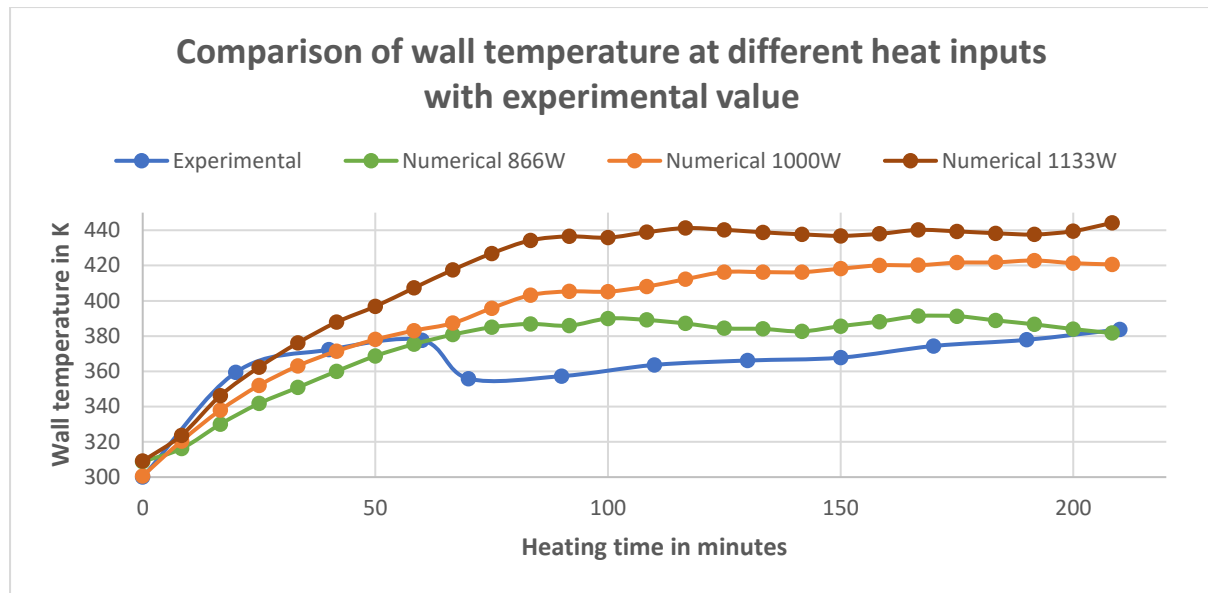


Figure 4.4: Temperature analysis of the wall under varying heat inputs and compared with experimental results

4.3 Temperature variation on different surfaces in the receiver

The *Figure 4.5* presented below illustrates the temperature variation on different surfaces over time. Notably, the back wall exhibits the highest temperature among all surfaces. This is primarily because solar radiation directly falls on the back wall, resulting in its significant heating. The heated back wall subsequently transfers heat to the surrounding air, cookies, and receives additional solar radiation.

The side walls, which are initially at relatively lower temperatures, gradually heat up due to the influence of the heated air and back wall. Atmospheric air enters the receiver through a hole located beneath the glass mouth, where it gradually warms up through direct solar radiation and convective heat transfer from the heated walls. As a result, the cookies' temperature increases due to the influence of the heated air and the direct solar radiation they receive.

The glass positioned at the mouth of the receiver plays a role in allowing heat to enter the interior of the receiver while simultaneously experiencing an increase in its own temperature. However, the glass maintains the minimum temperature among all the surfaces of the receiver due to its direct heat loss to the surrounding environment.

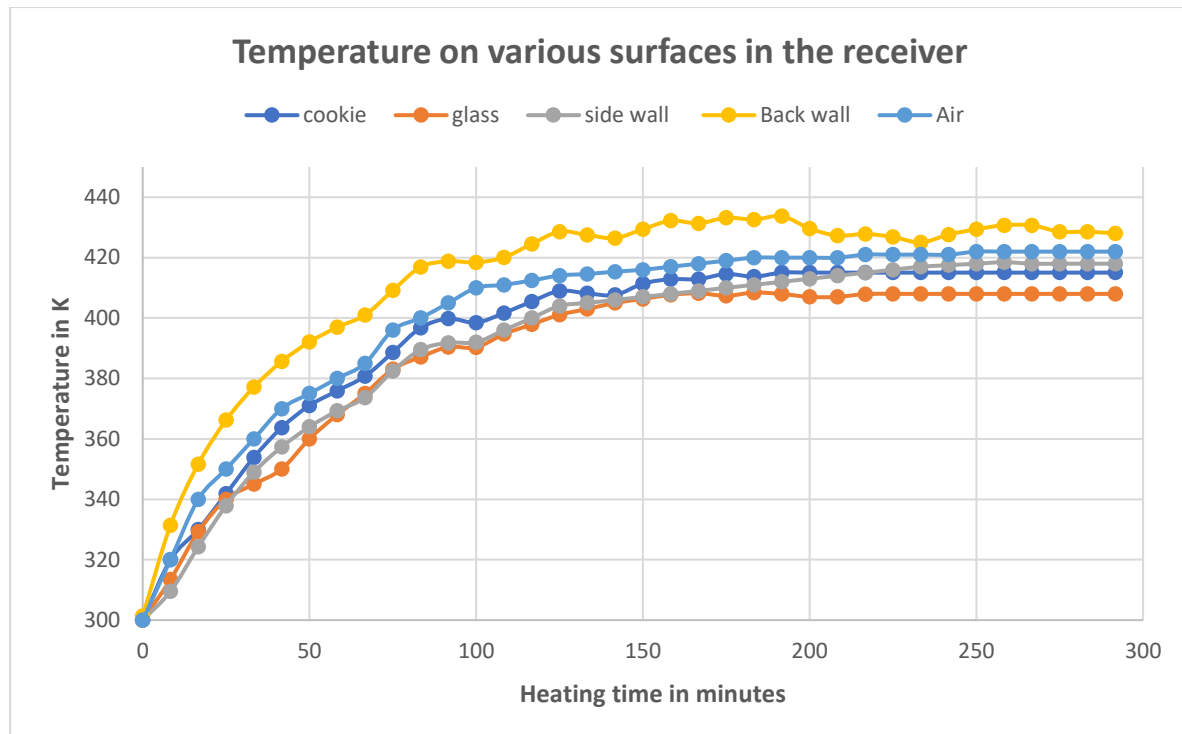


Figure 4.5: Variation of temperature on different surfaces of receiver

4.4 Energy losses and energy absorbed in receiver

The provided Figure 4.6 illustrates the different types of losses in the receiver, specifically convective heat transfer and radiative heat transfer. It is observed that the maximum radiative loss occurs from the wall, as it attains the highest temperature. Another radiative loss occurs from the glass, but its value is lower compared to the radiative loss from the wall due to the glass's relatively lower temperature.

Convective loss occurs in two forms. Firstly, there is convective mass transfer through the hole located at the top wall of the receiver. This loss is a result of the heated air carrying away energy at a temperature of 420K, intentionally provided for the evaporation of water. Secondly, there is convective loss from the glass surface that is in contact with the ambient environment. The outer surface of the glass, at a temperature of 400K, creates a convective flow that transfers heat to the surrounding ambient environment at 300K.

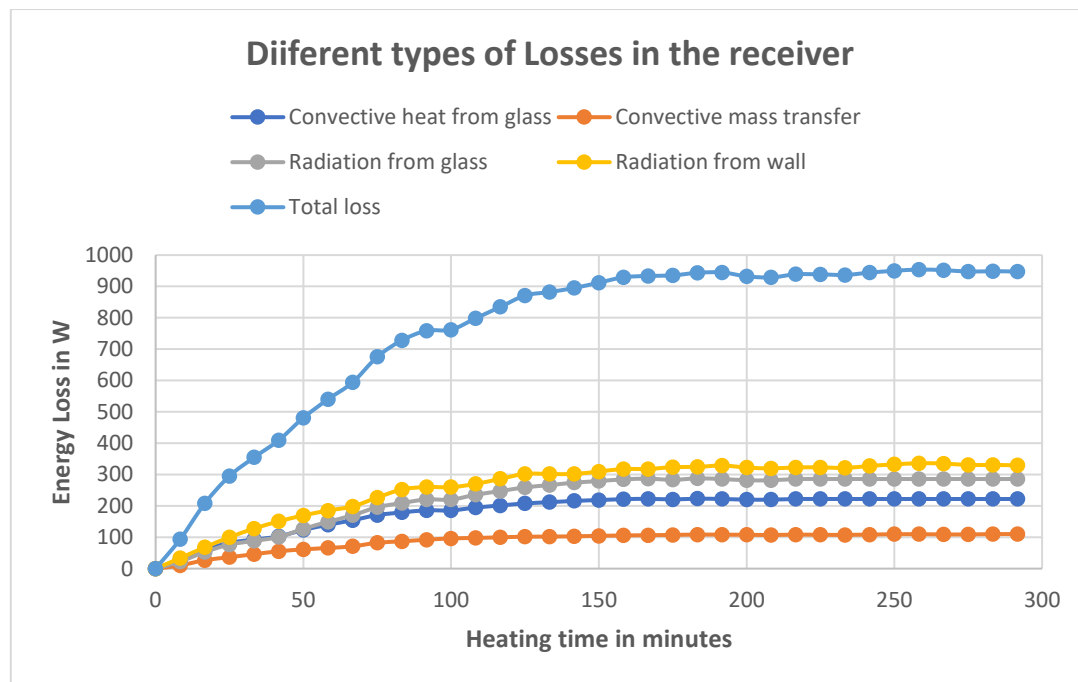


Figure 4.6: Variation of Different types of losses in the receiver with heating time

The Figure 4.7 provided illustrates the heating energy required to increase the temperature of various surfaces in the receiver, including cookies, walls, and glass. Based on the given information, we can conclude that the walls of the receiver require the maximum amount of energy. This is primarily due to their high mass, which is approximately 12 kg.

The cookies, with a mass of 3 kg, consume around 80 kJ of energy until they reach their steady state temperature. On the other hand, the glass surface requires the minimum amount of energy, as it has a relatively lower weight compared to the other surfaces.

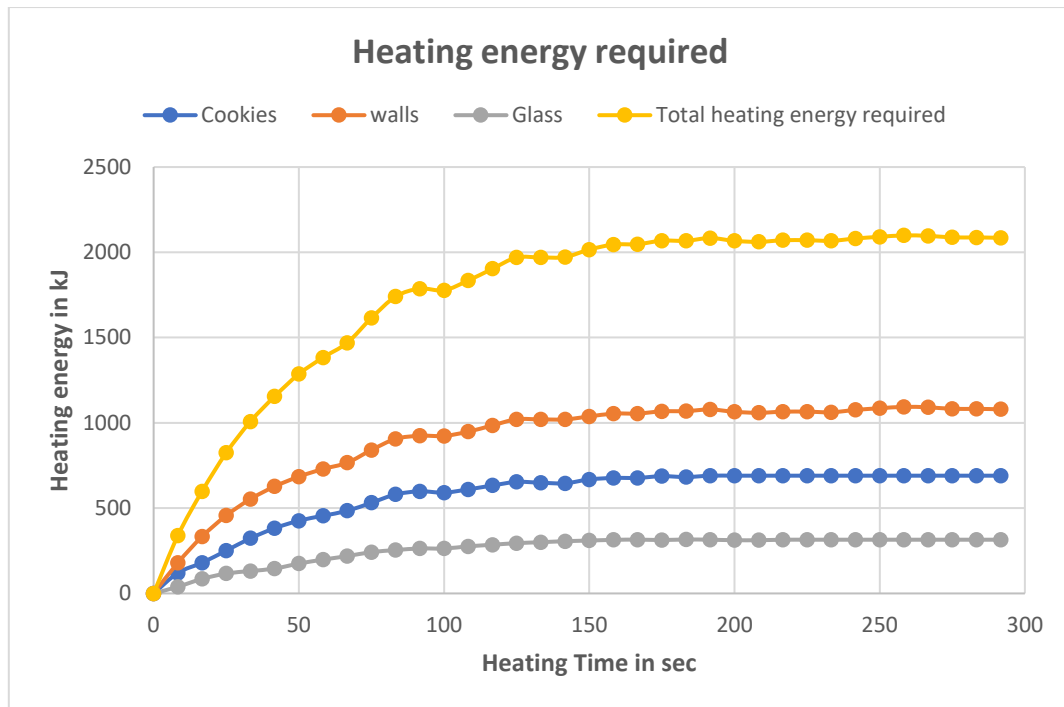


Figure 4.7: Variation of heating energy required for cookies, glass and walls with heating time

The provided Figure 4.8 illustrates the relationship between the energy required for heating cookies, glass, and walls, as well as the loss of heat energy over time. It accurately demonstrates that the heating energy decreases as time progresses, reflecting the increase in temperature of the cookies, glass, and walls. This rise in temperature leads to a decrease in the heat transfer rate.

The energy loss experienced in the system is influenced by the temperatures of the cookies, glass, and walls. As the temperature increases, the heat losses also increase. The figure effectively portrays this correlation. It is important to note that the sum of both heating energy and heat loss is equal to the total energy input.

When the system reaches a steady state, the heating energy required approaches zero, indicating that all the input energy is dissipated as heat loss. This behaviour is correctly represented in the figure.

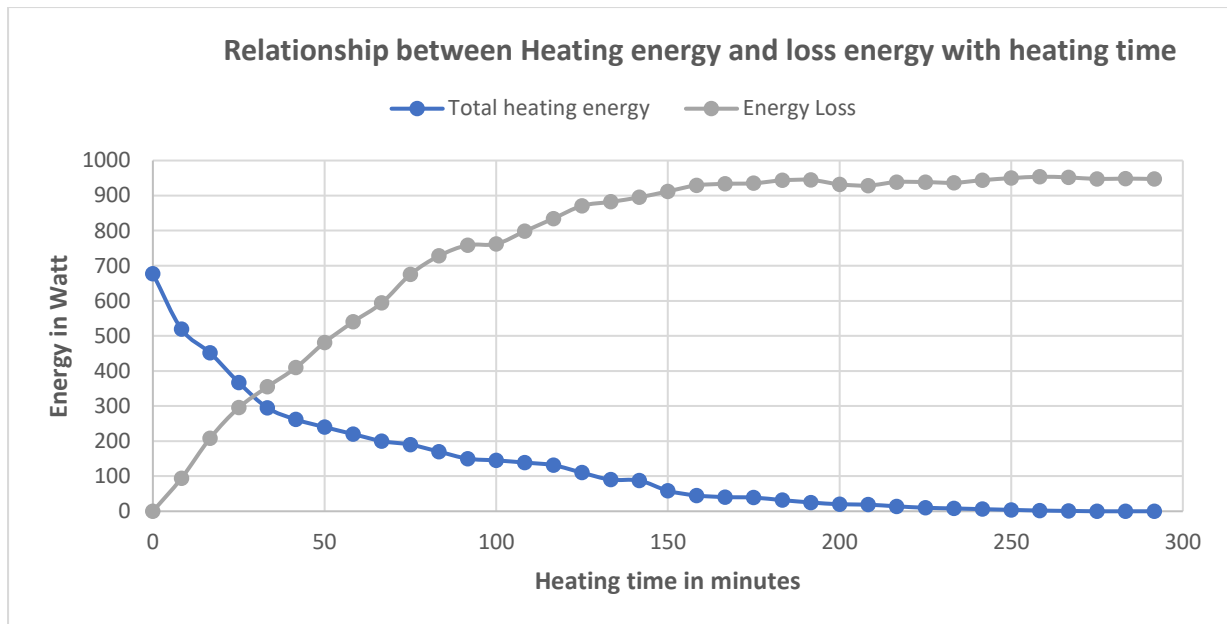


Figure 4.8: Relationship between variation of total heating energy and heat loss with time

This chapter deals with the results and discussions having comparison between experimental and numerical results, temperature contours and energy losses and energy absorbed in receiver.

Chapter 5

Conclusion and Future Plan

5.1 Conclusion

Baking process is one of the main energy consuming processes which includes different changes that are mostly time and temperature dependent at various stages. Moisture and heat transfer processes like convection, radiation and conduction plays important role in baking dough for getting quality product. The analysis involved studying the temperature variations of cookies, walls, and glass surfaces under different heat inputs (866W, 1000W and 1135W). The findings demonstrate that the temperature variation of the cookie at an input of 1000W closely resembles the experimental results with deviation of less than 5% for the cookie and 14% for the wall. The study found that the back wall of the receiver experienced the highest temperature due to direct solar radiation, while the side walls and cookies heated up gradually through convective heat transfer. In contrast, the glass surface, serving as an entry point for solar heat, exhibited the lowest temperature due to heat loss to the surrounding ambient environment.

Moreover, energy requirements revealed that as the temperature increased, the heat transfer rate decreased, leading to a decrease in the heating energy required. The energy loss in the system was influenced by the surface temperatures, with higher temperatures resulting in increased heat losses. Finally, at a steady state, the heating energy required approached zero, signifying that all input energy was dissipated as heat loss.

The report provides a comprehensive overview of the numerical analysis of a solar receiver for bakery applications using Ansys Fluent. Through the detailed description of the receiver's geometry, meshing techniques, boundary conditions, and computational modelling, we have gained valuable insights into

the performance and optimization of the system. The numerical analysis facilitated the accurate simulation of heat transfer, fluid flow, and energy balance within the receiver. By leveraging Ansys Fluent's capabilities, we were able to evaluate temperature distribution, energy absorption efficiency, and thermal performance. These findings contribute to the design and optimization of solar receivers tailored for bakery operations, enabling sustainable and efficient baking processes. The report underscores the importance of numerical analysis and simulation tools in designing and improving solar receivers, ultimately advancing the development of renewable energy solutions for bakery applications. These findings can guide the design and optimization of solar heating systems for bakery applications, enhancing energy efficiency and baking performance. The understanding of temperature distribution and energy requirements can aid in achieving uniform heating and efficient utilization of solar energy. Further research and development in this area can lead to advancements in sustainable baking technologies and contribute to a greener and more energy-efficient future.

5.2 Future Scope

1. It includes the possibility of conducting cooking modelling to analyse the temperature profiles and heat requirements for baking cookies. This modelling approach would also incorporate the energy needed for chemical reactions and evaporation processes occurring within the cookies.
2. The report focused on a specific set of heat inputs and boundary conditions. Conducting parametric studies can expand the scope of the analysis by investigating the effects of varying parameters such as solar radiation intensity, receiver geometry, and material properties. This will help in understanding the system's sensitivity to different factors and optimizing its performance accordingly.
3. The tracking requirements on the current prototype are such that one needs to be continuously available to track the collector manually and rotate the inner cage holding baking trays frequently. The tracking could either be automated or changes in receiver design could accommodate the same

References

- Al-Nehari, H.A., Mohammed, M.A., Odhah, A.A., Al-attab, K.A., Mohammed, B.K., Al-Habari, A.M. and Al-Fahd, N.H., 2021. Experimental and numerical analysis of tiltable box-type solar cooker with tracking mechanism. *Renewable Energy*, 180, pp.954–965. <https://doi.org/10.1016/j.renene.2021.08.125>.
- Food marketing technology, 2022. *Bakery Industry in India - The Prospect and Growth in near Future*. [online] Available at: <<https://fmtmagazine.in/bakery-industry-in-india/>> [Accessed 6 July 2022].
- Fortune business insights, 2022. *Bakery Products Market Size, Analysis & Growth Report [2028]*. [online] Available at: <<https://www.fortunebusinessinsights.com/industry-reports/bakery-products-market-101472>> [Accessed 6 July 2022].
- Statista, 2022. *Bread - India | Statista Market Forecast*. [online] Available at: <<https://www.statista.com/outlook/cmo/food/bread-cereal-products/bread/india?currency=USD>> [Accessed 6 July 2022].
- Dasanna Amit, 2022. *Homemade Bread | White Bread » Dassana's Veg Recipes*. [online] Available at: <<https://www.vegrecipesofindia.com/white-bread-easy-white-bread/>> [Accessed 9 July 2022].
- Lytfire, 2022. *Powerful Solar Oven & Roaster - Lytfire*. [online] Available at: <<https://lytfire.com/powerful-solar-oven-roaster>> [Accessed 11 July 2022].
- Ayub, I., Munir, A., Amjad, W., Ghafoor, A. and Nasir, M.S., 2018a. Energy- and exergy-based thermal analyses of a solar bakery unit. *Journal of Thermal Analysis and Calorimetry*, 133(2), pp.1001–1013. <https://doi.org/10.1007/s10973-018-7165-3>.
- Ayub, I., Munir, A., Ghafoor, A., Amjad, W. and Nasir, M.S., 2018b. Solar Thermal Application for Decentralized Food Baking Using Scheffler Reflector Technology. *Journal of Solar Energy Engineering, Transactions of the ASME*, 140(6). <https://doi.org/10.1115/1.4040206>.

- Davidson, I., 2016. *Biscuit baking technology: processing and engineering manual*. Academic press.
- Gruber, A., 2013. *711.4 (Energy) Energizing Sustainable Cities*. [online] London: Routledge. Available at: <<https://www.routledge.com/Energizing-Sustainable-Cities-Assessing-Urban-Energy/Grubler-Fisk/p/book/9781849714396>> [Accessed 6 July 2022].
- Jagtap, S., Kedare, S.B. and Modi, A., 2021. *Development and Testing of a Small Solar Bakery*.
- Jagtap, S.K., Kedare, S.B. and Modi, A., 2022. *Development and Testing of a Small Solar Bakery*.
- Jilte, R.D., Kedare, S.B. and Nayak, J.K., 2013. Natural Convection and Radiation Heat Loss from Open Cavities of Different Shapes and Sizes Used with Dish Concentrator. *Mechanical Engineering Research*, 3(1), p.25. <https://doi.org/10.5539/mer.v3n1p25>.
- Mishra, A., Powar, S. and Dhar, A., 2019. Solar Thermal Powered Bakery Oven. In: *Energy, Environment, and Sustainability*. Springer Nature. pp.577–592. https://doi.org/10.1007/978-981-13-3302-6_19.
- Paitoonsurikarn, S., Taumoeafolau, T. and Lovegrove, K., 2003. *Investigation of Natural Convection Heat Loss from a Solar Concentrator Open Cavity Receiver at Varying Angle of Declination*. [online] Available at: <<http://www.asme.org/about-asme/terms-of-use>>.
- Malhotra, K.S., Nahar, N.M. and Rao, B.R., 1983. *Optimisation factor of solar ovens*. *Solar Energy*, 31(2), pp.235-237.
- Singh, P.K. and Kondeti, B.I., 2020. Solar Bakery Oven Solar Bakery Oven View project Energy Storage Systems for Electric Vehicles View project. [online] <https://doi.org/10.13140/RG.2.2.35828.99200>.
- Telkes, M., 1959. Solar cooking ovens. *Solar Energy*, 3(1), pp.1-11.

Acknowledgments

I would like to express my sincere gratitude to all individuals and organizations who have contributed to the successful completion of this report.

First and foremost, I extend my deepest appreciation to **Prof. S. B. Kedare**, my guide, and also **Prof. Manaswita Bose** for their guidance, valuable insights, and unwavering support throughout the project. Their expertise and mentorship have been instrumental in shaping the direction and quality of this report.

I would also take this opportunity to thank other faculty members at the department for the attitude they helped develop in scientific research and senior doctoral students especially **Mr. Shivam Kumar** and **Mr. Indranil Paul** from the 'Sustainable Development' lab for their help.

Lastly, I extend my heartfelt appreciation to my friends and family for their constant encouragement and support throughout this endeavour.

The successful completion of this report would not have been possible without the collective effort and support of all those mentioned above. I am truly grateful for their contributions and the positive impact they have had on this project.